Dynamics of a cw multimode dye laser

J. Sierks, T. J. Latz, V. M. Baev, and P. E. Toschek
Institut für Laser-Physik, Universität Hamburg, D-20355 Hamburg, Germany
(Received 10 September 1997)

The spectral and temporal dynamics of a multimode dye laser has been studied theoretically and experimentally. The analytical model includes quantum fluctuations as well as *four-wave mixing* due to population pulsations, stimulated Brillouin scattering, and Rayleigh scattering both in a standing-wave linear laser, and in a unidirectional ring laser. The nonlinearity found most important in the multimode dye laser is four-wave mixing due to *pulsations of the population* of the upper laser level. Numerical simulations show features that characterize this particular type of mode coupling: broadening of the emission spectrum, oscillations of the light flux in individual laser modes, suppression of certain beat notes. Observations of these features confirm population pulsations dominating the laser dynamics. Four-wave mixing due to population pulsations tends to arrange the phases of the laser modes such as to minimize the pulsations and to limit its own strength. [S1050-2947(98)08103-7]

PACS number(s): 42.55.Mv, 42.60.Mi, 42.65.Es, 42.65.Sf

I. INTRODUCTION

The emission spectra of multimode lasers are very sensitive to absorption inside the laser cavity [1–3]. Perturbation of the laser emission dynamics by quantum noise and nonlinear mode coupling limits the sensitivity. Such a limitation impedes the applicability of intracavity absorption for a powerful spectroscopic technique (intracavity absorption spectroscopy, ICAS). Reduction of these perturbations would require a detailed knowledge of their origin and their influence on multimode lasers dynamics, which has not been studied exhaustively so far.

This paper presents a theoretical model for the dynamics of the light field in a cw multimode dye laser including quantum noise and mode coupling that originates from four-wave mixing (FWM) due to population pulsations (PP) on the upper laser level, and due to stimulated Brillouin scattering (SBS). The model is applicable to most types of lasers with homogeneously broadened gain, and, even with minor modifications, to those lasers with inhomogeneously broadened gain that emit within a bandwidth much narrower than the homogeneous broadening.

The results of numerical simulations are found to be in good agreement with experimental data on the spectral dynamics of a multimode Rh6G dye laser, recorded at high spectral and time resolution. The emission spectrum of a dye laser shows the highest sensitivity to intracavity absorption achieved so far [4,5]. As a result, it reacts also sensitively to various perturbations [6–8], and can be conveniently used to monitor weak mode coupling.

A very important contribution to FWM in a multimode laser is the modulation of the gain in frequency and spatial domain due to saturation by interfering laser modes. This phenomenon was predicted by third-order laser theory [9]. Saturation of the inversion takes place mainly as a depletion of the upper laser level. The lower-level lifetime is shorter by more than one order of magnitude than that of the upper laser level, such that its occupation is negligible. Gain saturation causes PP of the upper laser level with the mode-separation frequency, as well as spatial hole burning, which is in fact a product of degenerate PP at zero frequency. The two effects yield nondegenerate and degenerate FWM of laser modes.

So far, equations of motion of the multimode laser field have been solved analytically for up to three modes. Lasers that are used for intracavity spectroscopy, however, may show ten through several thousand oscillating modes. Equations for 500 oscillating modes have been solved numerically for a unidirectional ring laser [10]. The influence of PP back on the intermode beat notes was shown to be destructive, and self-limitation of PP was predicted. However, that model has substantial restrictions: it did not include quantum noise, the calculations were performed only on a time scale too short for reaching a stationary distribution of the light power among the modes, and intracavity absorption lines were replaced by sinusoidal modulation of spectral loss. The stationary distribution of the laser emission was also calculated [11]; though with certain oversimplifications: only 30 modes were assumed to be oscillating, and a fake etalon reduced their number to three in the stationary state. These results seem inapplicable to comparison with the stationary operation of a real multimode laser with intracavity absorption.

Another important contribution to FWM in a dye laser might arise from the nonlinearity of the dye solution, in particular from stimulated Raman, Rayleigh, Rayleigh wing, and Brillouin scatterings. An incident pair of light waves with different frequencies generates a material excitation at its beat frequency; in turn, the material excitation interacts with each of the incident waves and induces a dielectric polarization whose frequency is shifted away from that of the incident waves by the beat frequency. This coupling generates FWM of the light waves. The process may be modeled by perturbation theory [12,13]. If only two waves are present, the FWM is degenerate. In a multimode laser, however, there are many light waves of different frequencies corresponding to the longitudinal cavity modes. Each pair of these light waves reads out material excitations, created by *all other* pairs of light waves with the same beat frequency. Hence stimulated scattering in a multimode laser causes degenerate and nondegenerate FWM.

Nonlinear light scattering can be caused by various material excitations. Some of them have resonance frequencies on the order of the mode beat frequency, and therefore strongly influence the mode coupling. SBS, e.g., is caused by acoustic phonons produced via the electrostrictive effect [14]. Stimulated Rayleigh wing scattering is the result of libration of the orientation of anisotropic molecules of the solvent. The strength of the Rayleigh wing scattering is proportional to the optical Kerr constant, whereas SBS is proportional to the electrostrictive constant. It was shown that in alcohols used as solvents for many dyes, the optical Kerr constant is about 20–30 times smaller than the electrostrictive constant [15]. Therefore we will neglect Rayleigh wing scattering as compared with SBS.

Other scattering mechanisms, such as stimulated Rayleigh scattering (SRLS) and stimulated Raman scattering (SRS), have resonance frequencies very different from intermode frequencies; they are less important for mode coupling. SRLS is the result of local fluctuations of density and temperature; it has its maximum close to zero frequency shift. Only a very small portion of this scattering in the far wings of its spectral profile may contribute to mode coupling. In the following we shall estimate the contribution of SRLS to the nonlinear mode coupling in the dye laser. In contrast, SRS is caused by the internal vibration or rotation in molecules with resonance frequencies that exceed the width of the emission spectrum of the laser. Moreover, its peak value is smaller than that of resonant SBS. Therefore, SRS is neglected too.

The only type of stimulated scattering so far considered to affect multimode dye lasers is SBS. Numerical simulations of the spectral dynamics of a $Rh6G$ dye laser under the influence of SBS have been carried out to determine the limitation of the sensitivity to intracavity absorption [16,17], and to explain chaotic laser dynamics [18]. The observed redshift and asymmetry of the emission spectra was ascribed to the Stokes part of SBS [19]. All simulations in these works were performed in terms of a simplified photon approach leaving out nondegenerate FWM. The strength of SBS usually served as a parameter specified by fitting the numerical results to the experimental data. Only linear lasers were considered, and SBS in the backward direction, where the frequency shift is large. However, a considerable redshift of the emission was observed even in unidirectional ring lasers [20], indicating small-angle scattering in the forward direction to appear.

The main purpose of this paper is to develop a model for an adequate description of the dynamics of the light amplitudes in a multimode dye laser by taking into account quantum fluctuations and the predominant mechanisms of FWM with realistic parameters, such that quantitative analysis and comparison with experiment become feasible. In Sec. II, the models for the description of FWM due to PP and stimulated Brillouin and Rayleigh scattering are introduced. Here, SBS is taken into account, both in backward and forward directions, by considering the transverse spatial mode profile. The contribution of optothermally excited phonons to Brillouin and Rayleigh scattering, known to appear in absorbing liquids [21], is also estimated. Section III is devoted to an analysis of numerical simulations with the help of the model. The data show the spectral dynamics of the emission of multimode lasers under the influence of SBS or PP. They reveal the qualitative difference between FWM of saturation type, which is represented by PP, and of stimulated-scattering type, which is represented by SBS. The influence of simultaneous PP and SBS on the spectral dynamics of the laser is studied. In Sec. IV the spectrum of beat notes, the source of FWM, is studied in the presence of PP and SBS. Analytical and numerical calculations of the model are supplemented by results of measurements of the dynamics of emission spectra and beat notes. In Sec. V the main results are summarized.

II. MODEL OF A MULTIMODE DYE LASER INCLUDING FOUR-WAVE MIXING

A. Susceptibility

We assume that light is emitted into many longitudinal laser modes that are associated with only one fundamental transverse mode of linear polarization. The eigenfrequencies of these laser modes are multiples of the cavity's free spectral range $\delta\omega$,

$$\omega_q = q\,\delta\omega, \tag{1}$$

where q is any positive integer. The electric field $\mathbf{E}$ of the electromagnetic light wave inside the cavity can be expanded in the electric-field amplitudes of the cavity modes,

$$\mathbf{E} = \tfrac{1}{2}\sum_q \mathbf{E}_q(t,\mathbf{x})\exp(-i\omega_q t) + \mathbf{E}_q^*(t,\mathbf{x})\exp(i\omega_q t). \tag{2}$$

The dielectric polarization $\mathbf{P}$ induced by the light field has the same frequency as the light and can be expanded into the same frequency components,

$$\mathbf{P} = \tfrac{1}{2}\sum_q \mathbf{P}_q(t,\mathbf{x})\exp(-i\omega_q t) + \mathbf{P}_q^*(t,\mathbf{x})\exp(i\omega_q t). \tag{3}$$

Here the complex amplitudes $\mathbf{P}_q$ and $\mathbf{E}_q$ are slowly varying functions of time on the scale of one cavity round trip, $2\pi/\delta\omega$.

The dielectric polarization $\mathbf{P}$ generated by $\mathbf{E}$ derives from the susceptibility tensor χ, which is usually expanded into a power series of the electric field. In general, the spatial components of the polarization vector can be expressed [22] as

$$P_i(\omega_i) = \varepsilon_0(\chi_{ij}^{(1)}E_j + \chi_{ijk}^{(2)}E_jE_k + \chi_{ijkl}^{(3)}E_jE_kE_l + \cdots). \tag{4}$$

A dye solution is a homogeneous medium with inversion symmetry. Therefore we shall neglect $\chi^{(2)}$ and assume that the tensor $\chi^{(3)}$ is diagonal, i.e., we neglect the vectorial nature of light and write only one component E of the electric field, and one component P of the polarization. Then the lowest-order nonlinear term in Eq. (4) is $\chi^{(3)}E^3$, with $\chi^{(3)}$ being the corresponding component of the susceptibility tensor. After expanding P and E in the frequency components of the cavity modes by Eqs. (2) and (3), we keep only the polarization terms having frequencies that coincide with one of the laser modes. Since all four light frequencies are represented by light waves from within a laser emission bandwidth which is much smaller than the central emission frequency, one of the three light frequenciesin the product E^3,

on the right-hand side of Eq. (4), must have its sign opposite to the signs of the other two frequencies. For complex polarization and field amplitudes at the frequency ω_q, we obtain the relation

$$P_q=\varepsilon_0\left(\chi^{(1)}_{q,q}E_q+\tfrac{1}{2}\sum_r\sum_p\chi^{(3)}_{q,-(p+r),p,q+r}E^*_{p+r}E_pE_{q+r}\right). \tag{5}$$

Here q and p are positive integers, and r is the difference between indices of two oscillating laser modes, which is any integer, positive and negative, satisfying the condition $|r|\ll q,p$. The sum in Eq. (5) extends over all possible combinations of oscillating modes.

The linear susceptibility $\chi^{(1)}$ is proportional to a density $\rho^{(0)}$, unmodified by light, which may represent the mass density of the solvent, or the unsaturated inversion density of the laser dye. The interference, or beating, of two light waves $E^*_{p+r}E_p$ induces a deviation $\rho^{(2)}$ from the unperturbed density $\rho^{(0)}$ that gives rise to a third-order contribution to the susceptibility. SBS takes place with deviations from the mass density (''phonons''), and PP represent periodic deviations from inversion density. The most natural way of expanding these deviations $\rho^{(2)}$ is in a Fourier series that contains all intermode beat frequencies. The total density ρ is then written as

$$\rho=\rho^{(0)}+\sum_r\rho^{(2)}_r\exp(-i\omega_r t)=\rho^{(0)}+\langle\rho^{(2)}_0\rangle_z+\Delta\rho^{(2)}=\langle\rho\rangle_{z,t}+\Delta\rho^{(2)}, \tag{6}$$

where $\rho^{(2)}_r$ is the deviation of the density at the frequency ω_r, resulting from all pairs of light waves separated by that frequency and numbered by the index p, and z is the coordinate along the optical axis. We have separated the deviations $\rho^{(2)}$ into a constant part $\langle\rho^{(2)}_0\rangle_z$ that is proportional to the light intensity, and an oscillating part $\Delta\rho^{(2)}$ with Fourier components $\Delta\rho^{(2)}_r=\rho^{(2)}_r-\delta_{r,0}\langle\rho^{(2)}_0\rangle_z$. The constant part $\langle\rho^{(2)}_0\rangle_z$, combined with the unperturbed density $\rho^{(0)}$, is written $\langle\rho\rangle_{z,t}$. It represents the mean mass density of solvent or saturated inversion density *modified* by the light. The second part $\Delta\rho^{(2)}_r$ includes oscillating terms with values depending on the actual distribution of the light intensity among the modes.

Spatial and temporal deviations of the total light intensity from its mean value are small, since they are averaged over many modes. As a result, the deviations $\Delta\rho^{(2)}_r$ of the density from the mean value $\langle\rho\rangle_{z,t}$ are also small. Therefore the polarization in Eq. (5) can be expressed as

$$P_q=\varepsilon_0 C\left(\langle\rho\rangle_{z,t}E_q+\sum_r\Delta\rho^{(2)}_{-r}E_{q+r}\right), \tag{7}$$

where C is the linear susceptibility per density, and we consider $\Delta\rho^{(2)}_r$ the perturbation. This approach differs from the usual perturbative approach, and is particularly fitting since its validity does not explicitly require small light intensities. It especially suits multimode lasers, where the intensity in individual modes exhibits full-scale fluctuations, whereas the total intensity is constant.

Now the frequency component of the density deviations $\Delta\rho^{(2)}_r$ can be expanded into plane waves,

$$\Delta\rho^{(2)}_r=\Delta\rho^{(2)*}_{-r}=\frac{1}{\sqrt{(2\pi)^3}}\int d^3\mathbf{K}\;\Delta\rho^{(2)}_{r,\mathbf{K}}\exp(i\mathbf{K}\cdot\mathbf{r}), \tag{8}$$

where $\mathbf{r}$ is a spatial vector, $\mathbf{K}$ is the vector of the density wave, and

$$\Delta\rho^{(2)}_{r,\mathbf{K}}=\frac{F_r(|\mathbf{K}|^2)}{\sqrt{(2\pi)^3}}\int d^3\mathbf{r}\sum_p\tfrac{1}{2}(E^*_pE_{p+r}-\delta_{r,0}\langle E^*_pE_p\rangle_z)\times\exp(-i\mathbf{K}\cdot\mathbf{r}) \tag{9}$$

are expansion coefficients. Here, $F_r(|\mathbf{K}|^2)$ is the function of the density response to the light field determined from the nonlinear susceptibility by Eqs. (5)–(9). The response function entails both electronic *and* center-of-mass excitation. The Kronecker symbol $\delta_{r,0}$ takes into account subtraction of the total laser intensity in accordance with our particular perturbative approach. The integral in Eqs. (8) is taken over all three wave-vector coordinates (K_x,K_y,K_z), and the integral in Eq. (9) is taken over all three spatial coordinates of $\mathbf{r}(x,y,z)$.

In the above terminology, the deviations of the density induced by two light waves depend only on the beat frequency ω_r, on the absolute difference of the wave vectors, and on the response function $F_r(|\mathbf{K}|^2)$.

B. Mode geometry

Light propagation in nonlinear dielectric media is governed by the inhomogeneous electromagnetic wave equation

$$\boldsymbol{\nabla}\times\boldsymbol{\nabla}\times\mathbf{E}+\frac{n^2}{c^2}\frac{\partial^2\mathbf{E}}{\partial t^2}=-\frac{1}{\varepsilon_0c^2}\frac{n^2+2}{3}\frac{\partial^2\mathbf{P}}{\partial t^2} \tag{10}$$

derived from Maxwell's equations. The correction factor $(n^2+2)/3$ takes into account the effect of the local field [23]. This formulation requires that $\mathbf{P}$ excludes linear refraction, because n has been inserted directly into the electromagnetic wave equation instead of arising from $\mathbf{P}$, when deriving Eq. (10).

The restriction to a scalar field leaves only one component of electric field E and polarization P. The electric-field amplitude in the laser modes is expressed by the reduced amplitudes a_q ($M_q=a^*_qa_q$ is the number of ''photons'' in the mode q), and a spatial eigenfunction Ψ_q:

$$E_q=\left(\frac{2\hbar\omega_q}{n^2\varepsilon_0}\right)^{1/2}a_q(t)\Psi_q(\mathbf{x}). \tag{11}$$

In the approximation of slowly varying amplitudes [9], the reduced amplitudes in Eq. (10) are driven by the dielectric polarization in the laser cavity according to

$$\frac{d}{dt}a^{(P)}_q=\frac{i\omega_q}{2\varepsilon_0}\frac{n^2+2}{3n^2}\left(\frac{n^2\varepsilon_0}{2\hbar\omega_q}\right)^{1/2}\int d^3\mathbf{r}\;\Psi^*_qP_q. \tag{12}$$

Here, the last factor is a spatial overlap integral of polarization and light amplitudes.

We now consider the nonlinear part of the polarization only, i.e., the third-order part given by the second term in Eq. (7). Substituting the density deviations by Eqs. (8) and (9), and the light amplitude by Eq. (11), and taking into account that the polarization outside the gain medium is zero, yields the third-order equation for the reduced amplitudes

$$\frac{d}{dt}\,a_q^{(3)}=\frac{i\omega_L}{2}\,\frac{n^2+2}{3n^2}\,\frac{\hbar\omega_L}{n^2\varepsilon_0}\,C\sum_r\,\sum_p\,a_{q+r}a_{p+r}^*a_p \times\int_{\substack{\text{gain}\\ \text{medium}}} d^3\mathbf{r}\;\Psi_q^*\Psi_{q+r}(\mathbf{r})\,\frac{1}{(2\pi)^3} \times\int d^3\mathbf{K}\;F_{-r}(|\mathbf{K}|^2)\int d^3\mathbf{r}'[\Psi_{p+r}^*\Psi_p(\mathbf{r}') -\delta_{r,0}\langle\Psi_p^*\Psi_p(\mathbf{r}')\rangle_z]\exp[i\mathbf{K}\cdot(\mathbf{r}-\mathbf{r}')]. \tag{13}$$

Here, by replacing the electric field amplitudes with Eq. (11), we assume the same frequency ω_L for all laser modes. Since the width of the emission spectrum, which limits $r\,\delta\omega$, is much smaller than the light frequency ω_L, this approximation is well justified. Equation (13) shows explicitly that the dynamics of individual laser modes of a multimode laser with a nonlinear medium in the cavity depends upon triple products of oscillating laser modes that represent four-wave mixing.

A specific calculation requires the substitution of expressions for the spatial eigenfunctions of the laser modes. We assume that the cavity extends from $z=0$ through $z=L$. The polarization is located in the gain medium of length l placed in the waist of the cavity mode at $z=z_g$, (with a ring cavity $z_g=0$). We shall assume the gain medium to be much longer than the wavelength of laser emission, but much shorter than the cavity length divided by the number of oscillating modes,

$$\frac{2\pi c}{n\omega_L}\ll l\ll\frac{L}{r}. \tag{14}$$

This condition holds for a typical cw dye laser.

Near the waist at z_g the wave is plane, and $\Psi_q(\mathbf{r})$ separates into a transverse part $\Omega(x,y)$ and the longitudinal one $Z_q(z)$:

$$\Psi_q(\mathbf{r})=\Omega(x,y)Z_q(z). \tag{15}$$

The z integral of $Z_q^*Z_q$ and the area integral of $\Omega^*\Omega$ are normalized to unity. Hermite-Gaussian TEM_{00} modes [24] are assumed for the transversal distribution,

$$\Omega=\left(\frac{2}{\pi w_0^2}\right)^{1/2}\exp\left(-\frac{x^2+y^2}{w_0^2}\right), \tag{16}$$

with w_0 being the radius of the waist of the electric field at the $1/e$ level. Since the transverse part of the spatial eigenfunction does not depend on the mode index q, the interference term of the spatial eigenfunctions of two different longitudinal modes $\Psi_p^*\Psi_{p+r}$ in Eq. (13) has the same transverse distribution as the intensity in the laser, $\Omega^*\Omega$. As in Eq. (8), we expand this distribution into plane waves,

$$\Omega^*\Omega=\frac{1}{(2\pi)^2}\int dK_x\int dK_y\,\exp\left[-\frac{w_0^2}{8}\,(K_x^2+K_y^2)\right] \times\exp[i(K_xx+K_yy)]. \tag{17}$$

The longitudinal part of the spatial eigenfunctions has two contributions corresponding to electromagnetic waves propagating in opposite directions, with wave vectors $\pm(n/c)\omega_q$ $Z_q^{\rightarrow}$ and $Z_q^{\leftarrow}$. They are related as

$$Z_q^{\rightarrow}=Z_q^{\leftarrow *}=\left(\frac{1}{L}\right)^{1/2}\exp\left(i\,\frac{n}{c}\,\omega_q z\right). \tag{18}$$

In unidirectional ring cavities, only copropagating pairs of travelling waves are excited. Their interference terms

$$Z_{p+r}^*Z_p=\frac{1}{L}\exp\left(-i\,\frac{n}{c}\,\omega_r z\right) \tag{19}$$

show small wave vectors that correspond to the beat note ω_r.

In standing-wave cavities the longitudinal part of the spatial eigenfunctions is

$$Z_q=\frac{1}{\sqrt{2}i}\,(Z_q^{\rightarrow}-Z_q^{\leftarrow})=\left(\frac{2}{L}\right)^{1/2}\sin\left(\frac{n}{c}\,\omega_q z\right). \tag{20}$$

The interference of two waves in a standing-wave cavity has two types of components: One, $Z_{p+r,p}^{2\Rightarrow}$, with small wave numbers $n\omega_r/c$ due to copropagating pairs of waves, as in the ring laser, and another, $Z_{p+r,p}^{2\leftrightarrow}$, with large wave numbers $n\omega_{2p+r}/c$, due to counterpropagating pairs of waves,

$$Z_{p+r}^*Z_p=\frac{1}{2L}\left[\exp\left(-i\,\frac{n}{c}\,\omega_r z\right)-\exp\left(-i\,\frac{n}{c}\,\omega_{2p+r}z\right)\right]+\text{c.c.} =Z_{p+r,p}^{2\Rightarrow}-Z_{p+r,p}^{2\leftrightarrow}. \tag{21}$$

The radius of the beam waist in a typical cw dye laser is much larger than the wavelength of the laser light, but much smaller than the wavelength of the *beat notes* of two laser modes. As a consequence, the relations

$$\left(\frac{n\omega_{2p+r}}{c}\right)^2\approx\left(\frac{2n\omega_L}{c}\right)^2\gg\langle K_x^2+K_y^2\rangle=\frac{8}{w_0^2}\gg\left(\frac{n\omega_r}{c}\right)^2 \tag{22}$$

hold. They indicate that counterpropagating pairs produce beat waves that propagate along the optical axis, but copropagating pairs of waves produce beat waves that propagate almost perpendicularly to the optical axis.

We insert Eq. (21) into Eq. (13) and perform the last two integrations. According to the condition in Eq. (14), we neglect integrals over fast oscillating terms, such as $\cos(2n\omega_Lz/c)$, across the dye jet. The result is split into two parts: one with a source term originating from counterpropagating waves, and another from copropagating pairs of waves. The former is

$$\frac{d}{dt}\,a_q^{(3,\leftrightarrow)}=\frac{i\omega_L}{2}\,\frac{n^2+2}{3n^2}\,\frac{\hbar\omega_L}{n^2\varepsilon_0}\,\frac{1}{\pi w_0^2}\,C \times\sum_r\,F_{-r}\left[\left(\frac{2n\omega_L}{c}\right)^2\right]a_{q+r}\sum_p\,a_{p+r}^*a_p\,\frac{l}{L^2} \times\int_{\substack{\text{gain}\\\text{medium}}}dz\,\frac{1}{l}\cos\left(\frac{n}{c}\,\omega_{2q+r}z\right)\cos\left(\frac{n}{c}\,\omega_{2p+r}z\right). \tag{23}$$

Here the response function of the density to the light field of plane beat waves, $F_r(|\mathbf{K}|^2)\approx F_r[(2n\omega_L/c)^2]$ is considered constant in the gain medium and is extracted from the integrals in Eq. (13), since the range of wave numbers of the beat notes is small, $r\,\delta\omega\ll 2\omega_L$ [Eq. (22)]. In contrast, nearly copropagating pairs of waves allow extraction of $F_r(|\mathbf{K}|^2)\approx F_r(K_x^2+K_y^2)$ only from the z and K_z integrals of Eq. (13). The equation Eq. (13), with source terms composed of copropagating waves, is

$$\frac{d}{dt}\,a_q^{(3,\Rightarrow)}=\frac{i\omega_L}{2}\,\frac{n^2+2}{3n^2}\,\frac{\hbar\omega_L}{n^2\varepsilon_0}\,C\sum_r\,\sum_p\,a_{q+r}a_{p+r}^*a_p\,\frac{l}{L^2} \times\left\{\left[\int_{\substack{\text{gain}\\\text{medium}}}dz\,\frac{1}{l}\cos^2\left(\frac{n}{c}\,\omega_r z\right)\right]-\delta_{r,0}\right\} \times\int\int dK_x dK_y F_{-r}(K_x^2+K_y^2) \times\exp\left[-\frac{w_0^2}{4}\,(K_x^2+K_y^2)\right]. \tag{24}$$

Equations (23) and (24) can be written in general form including copropagating and counterpropagating waves:

$$\frac{d}{dt}\,a_q^{(3,\leftrightarrow/\Rightarrow)}=\tfrac{1}{2}\sum_r\,S_r^{(\leftrightarrow/\Rightarrow)}a_{q+r}\sum_p\,a_{p+r}^*a_p(\xi_{p-q/r}^{(\leftrightarrow/\Rightarrow)} -\delta_{\leftrightarrow/\Rightarrow,\Rightarrow}\delta_{r,0}). \tag{25}$$

Here ξ denotes the results of the z integrals over the extension of the gain (from $z_g-l/2$ through $z_g+l/2$) in the spatial interference factors in Eqs. (23) and (24),

$$\xi_{p-q}^{(\leftrightarrow)}=\tfrac{1}{2}\,\operatorname{sinc}\left[\frac{\pi(p-q)l}{L}\right]\cos\left[\frac{\pi(p-q)2z_g}{L}\right], \tag{26}$$

$$\xi_r^{(\Rightarrow)}=\frac{1}{2}\left[1+\operatorname{sinc}\left(\frac{\pi rl}{L}\right)\cos\left(\frac{\pi r2z_g}{L}\right)\right]. \tag{27}$$

These integrals account for spatial correlations of the four interacting waves in the gain medium, and $\operatorname{sinc}(x)\equiv(\sin x/x)$. The Kronecker symbol $\delta_{r,0}$ is used for subtraction of the mean light intensity. In Eq. (25), all constants are lumped in the scattering coefficient S.

With the approximation of a thin gain medium [Eq. (14)], the sinc functions are close to unity. Moreover, with unidirectional ring cavities, $\xi_{p-r}^{(\leftrightarrow)}=0$ and $z_g=0$. In this case only one correlation term appears, $\xi_r^{(\Rightarrow)}=1$. With a symmetric standing-wave cavity (i.e., $z_g=L/2$), $\xi_r^{(\Rightarrow)}=[1+(-1)^r]/2$ and $\xi_{p-r}^{(\leftrightarrow)}=(-1)^{p-q}/2$. Thus all the odd modes in such a laser are correlated with each other, as well as all even modes. However, odd and even modes are uncorrelated with each other for copropagating pairs of waves, but anticorrelated for counterpropagating pairs of waves.

The scattering coefficient S should be determined individually for each type of FWM. In the next sections it will be calculated for nonlinearities that arise from population pulsations on the laser transition or from stimulated Brillouin and Rayleigh scattering.

C. Laser gain

The laser gain is obtained from a solution of the Maxwell-Bloch equations. For this purpose Eqs. (12), derived from Maxwell equations, must be combined with the equation for the material polarization,

$$P=D_{ab}(\rho_{ab}+\rho_{ba}). \tag{28}$$

We assume that the laser emission is resonant with transition $a\leftrightarrow b$ where $|a\rangle$ is the upper state; $|b\rangle$ the lower state; ω_{ab} the resonance frequency; D_{ab} the dipole matrix element; ρ_{ij} the density matrix, with $i,j\in\{a,b\}$; and $\rho_{ab}=\rho_{ba}^*$. We consider an ideal four-level dye laser whose relaxation rate of ground-state population density ρ_{bb} much exceeds the relaxation rate γ_a of the upper-state population density ρ_{aa}. Therefore we neglect ρ_{bb} and calculate the laser inversion by integrating ρ_{aa} over the gain medium,

$$N=\int_{z_g-l/2}^{z_g+l/2}dz\int_{-\infty}^{\infty}dx\int_{-\infty}^{\infty}dy\;\rho_{aa}. \tag{29}$$

The optical Bloch equations of motion for such a laser in the rotating-wave approximation, supplemented by rates of excitation and decay, are

$$\frac{d}{dt}\,\rho_{aa}=\Pi\,\frac{\Omega^2}{l}-\gamma_a\rho_{aa}-\frac{iD_{ab}}{2\hbar}\,\frac{n^2+2}{3}\left[\sum_q\,E_q^*\exp(i\omega_q t)\rho_{ab} -\text{c.c.}\right], \tag{30}$$

$$\frac{d}{dt}\,\rho_{ab}=-(i\omega_L+\gamma_t)\rho_{ab}-\frac{iD_{ab}}{2\hbar}\,\frac{n^2+2}{3}\sum_q\,\rho_{aa}E_q \times\exp(-i\omega_q t). \tag{31}$$

Here Π is the pump rate and γ_t is the dipole dephasing rate. Since in the dye laser $\gamma_t\gg\gamma_a$, Eq. (31) is adiabatically eliminated, i.e., it is replaced by the quasistationary solution

$$\rho_{ab}\approx-\frac{iD_{ab}}{2\hbar}\,\frac{n^2+2}{3}\,\rho_{aa}\sum_q\,\frac{E_q\exp(-i\omega_q t)}{i(\omega_L-\omega_q)+\gamma_t}, \tag{32}$$

and Eq. (30) writes

$$\frac{d}{dt}\rho_{aa}=\Pi\frac{\Omega^2}{l}-\rho_{aa}\left[\gamma_a+\left(\frac{D_{ab}}{2\hbar}\frac{n^2+2}{3}\right)^2\times\sum_q\sum_r\frac{E_q^*E_{q+r}\exp(-i\omega_r t)}{i(\omega_L-\omega_{q+r})+\gamma_t}+\text{c.c.}\right]. \quad (33)$$

The profile of the pump-light beam in a cw dye laser is usually adapted to that of the laser beam, such that we assume the distribution of the inversion density to agree with that of the laser intensity,

$$\rho_{aa}\approx\Omega^2(x,y)G, \quad (34)$$

where $G=\int_{-\infty}^{\infty}dx\int_{-\infty}^{\infty}dy\ \rho_{aa}$. With Eq. (34) taken into account, Eq. (33) is integrated over dx and dy and multiplied by Ω^2,

$$\frac{d}{dt}\rho_{aa}=\Pi\frac{\Omega^2}{l}-\rho_{aa}\left[\gamma_a+\left(\frac{D_{ab}}{2\hbar}\frac{n^2+2}{3}\right)^2\times\sum_q\sum_r\int\int dx\,dy\ \Omega^2\times\frac{E_q^*E_{q+r}\exp(-i\omega_r t)}{i(\omega_L-\omega_{q+r})+\gamma_t}+\text{c.c.}\right]. \quad (35)$$

The solution of Eq. (35) is cast in the form

$$\rho_{aa}=\langle\rho_{aa}\rangle_{z,t}+\Delta\rho_{aa}^{(2)}, \quad (36)$$

analogous to Eq. (6), with $\Delta\rho_{aa}^{(2)}$ compounded of the small second-order deviations of the inversion density from the mean value $\langle\rho_{aa}\rangle_{z,t}$ generated by temporal and spatial interference of laser modes.

We now consider the inversion $\overline{N}$ controlled by the mean light flux, i.e., temporally and spatially averaged. Spatial integration of Eq. (33) and temporal averaging yield according to Eqs. (11) and with the approximation

$$\left\langle\sum_q\sum_r\frac{E_q^*E_{q+r}\exp(-i\omega_r t)}{i(\omega_L-\omega_{q+r})+\gamma_t}+\text{c.c.}\right\rangle_{z,t}\approx\sum_q\frac{2\gamma_t}{(\omega_L-\omega_q)^2+\gamma_t^2}\frac{1}{l}\int_{z_g-l/2}^{z_g+l/2}dz\ E_q^*E_q, \quad (37)$$

the equation for the mean inversion [see Eq. (29)]

$$\frac{d}{dt}\overline{N}=\Pi-\gamma_a\overline{N}-\sum_q B_q\overline{Na}_q^*a_q, \quad (38)$$

where B_q is the rate of stimulated emission per inverted molecule and per photon. Its spectral profile is

$$B_q=\frac{B_{\max}}{1+[(\omega_q-\omega_L)/\gamma_t]^2}. \quad (39)$$

The maximum value of B_q at $\omega_q=\omega_L$ is determined from Eqs. (11) and (35)–(39) as

$$B_{\max}=\frac{\omega_L D_{ab}^2}{n^2\varepsilon_0\hbar\gamma_t}\left(\frac{n^2+2}{3}\right)^2\frac{1}{L}\int_{-\infty}^{\infty}dx\int_{-\infty}^{\infty}dy\ \Omega^4=\frac{\omega_L D_{ab}^2}{n^2\varepsilon_0\hbar\gamma_t L\pi w_0^2}\left(\frac{n^2+2}{3}\right)^2. \quad (40)$$

Note that the assumption of a Gaussian transversal distribution of the gain [Eq. (34)] results in $B_{\max}$ being half as large as the value calculated with a step function for the inversion density.

The stationary solution of the mean value of the inversion follows from Eq. (38),

$$\overline{N}=\frac{\Pi}{\gamma_a+\sum_q B_q a_q^*a_q}. \quad (41)$$

First-order equations for reduced amplitudes [Eq. (12)] are obtained by substituting the polarization from Eqs. (28) and (32), assuming $\rho_{aa}=\langle\rho_{aa}\rangle_{z,t}$, and adding terms that model cavity loss γ and quantum fluctuations

$$\frac{d}{dt}a_q^{(1)}=\frac{B_q\overline{N}-\gamma-c\kappa_q}{2}a_q+f_q. \quad (42)$$

Here κ_q is the coefficient of narrowband intracavity absorption, and f_q is a Langevin random force describing quantum noise that obeys the conditions [25]

$$\langle f_q(t)\rangle=0, \quad (43)$$

$$\langle f_p^*(t)f_q(t')\rangle=\gamma\delta(t-t')\delta_{p,q}. \quad (44)$$

The ratio of susceptibility over inversion density C in Eq. (7) is found by comparing the stimulated emission rate for light amplitudes $\frac{1}{2}B_qNa_q$ in Eqs. (40) and (42) with Eqs. (7) and (12),

$$C^{(\text{PP})}=\frac{-i3n^2l\pi w_0^2}{(n^2+2)\omega_L}B_q, \quad (45)$$

where the superscript stands for ''population pulsations''.

Approximate stationary solutions for the total ''photon number'' M and for the mean value of the inverse population are obtained from Eqs. (38) and (42) by neglecting f_q and assuming $\kappa_q=0$:

$$M=\sum_q a_q^*a_q\approx\frac{(\eta-1)\gamma_a}{B_{\max}}, \quad (46)$$

$$\overline{N}\approx\frac{\gamma}{B_{\max}}. \quad (47)$$

Here η is the pump rate relative to the laser threshold,

$$\eta=\frac{\Pi B_{\max}}{\gamma\gamma_a}. \quad (48)$$

With the definitions in Eqs. (39) and (40), the inversion density in Eq. (35) can be written as

$$\frac{d}{dt}\rho_{aa}=\frac{\eta\gamma\gamma_a}{B_{\max}}\frac{\Omega^2}{l}-\rho_{aa}\Bigg[\gamma_a+\sum_r\sum_q\frac{B_q+B_{q+r}}{2}\times a^*_{q+r}a_qLZ^*_{q+r}Z_q\exp(i\omega_r t)\Bigg]. \tag{49}$$

Subtraction of the zeroth-order equation for $\langle\rho_{aa}\rangle_{z,t}$ from Eq. (49), and dropping the products of second-order deviations, yields the equation of motion for the second-order contribution to the inversion density:

$$\frac{d}{dt}\Delta\rho^{(2)}_{aa}=-\Delta\rho^{(2)}_{aa}\Bigg(\gamma_a+B_{\max}\sum_q a^*_q a_q\Bigg)-\langle\rho_{aa}\rangle_{z,t}B_{\max}\sum_r\sum_q a^*_{q+r}a_q(LZ^*_{q+r}Z_q-\delta_{r,0})\times\exp(i\omega_r t). \tag{50}$$

Here the spectral variation of the gain coefficient B was neglected ($B_q\cong B_{\max}$). Fourier decomposition of Eq. (50) and insertion of the total photon number from Eq. (46) provides us, according to Eq. (9), with the response function

$$F_r(|\mathbf{K}|^2)=-\frac{\rho^{(0)}_{aa}B_{\max}}{\eta\gamma_a-i\omega_r}\frac{n^2\varepsilon_0}{\hbar\omega_L}. \tag{51}$$

This result shows that the response function for PP is *independent* of $\mathbf{K}$. The scattering coefficient S^{PP} for this nonlinearity can be found with Eqs. (24), (25), (45), and (47):

$$S_r^{(\mathrm{PP},\leftrightarrow)}=S_r^{(\mathrm{PP},\Rightarrow)}=-\frac{\gamma B_{\max}}{\eta\gamma_a+i\omega_r}. \tag{52}$$

This scattering coefficient has a Lorentzian spectral profile with width on the order of 100 MHz [half-width at half maximum (HWHM)] for a typical cw dye laser.

D. Phonons

In this section we consider the nonlinearity in the laser due to deviations of the density of the dye solution from its average value $\langle\rho\rangle_{z,t}$. The constant C in Eq. (7) relating the density of the dielectric material to the material's polarization is

$$C^{(\mathrm{SBS})}=\frac{n^2-1}{\rho_0}. \tag{53}$$

Since the main effect originating from density oscillations is stimulated Brillouin scattering for this constant we use the notation $C^{(\mathrm{SBS})}$ in order to distinguish it from the constant $C^{(\mathrm{PP})}$, determined by the nonlinearity of the gain, Eq. (45).

The solution of the coupled equations of motion for mass density and temperature [12] provides the response function

$$F_r(|\mathbf{K}|^2)=\frac{\frac{n^2-1}{2}\frac{n^2+2}{3}+\frac{\nu^2\beta_T}{C_p}\frac{\alpha cn}{i\omega_r-\Gamma_R}}{\omega_B^2\left(1+\frac{C_p-C_\nu}{C_p}\frac{\Gamma_R}{i\omega_r-\Gamma_R}\right)-\omega_r^2-i\omega_r\Gamma_B}\varepsilon_0|\mathbf{K}|^2. \tag{54}$$

Here β_T is the thermal expansion coefficient, ν is the speed of sound, C_p and C_ν are the specific heat capacities at constant pressure and constant volume, and α is the absorption coefficient. We assume that all the absorbed energy is thermalized immediately.

The denominator of the response function shows two resonances, at frequency shift $|\omega_r|=\omega_B$ and $\omega_r=0$. The first one is the Brillouin resonance, with

$$\omega_B=\nu|\mathbf{K}|=\frac{2\nu n\omega_L}{c}\sin\frac{\beta}{2}, \tag{55}$$

at which phase matching takes place of sound waves and the beat notes of the light, propagating at an angle β ($0\leqslant\beta\leqslant\pi$) to each other. The width of this resonance [full width at half maximum (FWHM)],

$$\Gamma_B=\frac{H}{\rho_0}|\mathbf{K}|^2, \tag{56}$$

is determined by the viscosity H of the solvent. The response varies over the Brillouin resonance within the frequency range

$$\omega_B\leqslant 2n\omega_L\nu/c=\omega_B^{\leftrightarrow}. \tag{57}$$

The maximum response of the Brillouin resonance $\omega_B^{\leftrightarrow}$ corresponds to density waves excited by counterpropagating light waves. Copropagating light waves in a unidirectional ring laser also excite Brillouin resonance, but with small frequencies determined by the divergence of the laser light in the cavity modes [Eq. (16)].

The second resonance is Rayleigh scattering at zero frequency with width (HWHM)

$$\Gamma_R=\frac{\lambda_T|\mathbf{K}|^2}{\rho_0 C_\nu}, \tag{58}$$

where λ_T is the thermal conductivity of the solvent.

The response function [Eq. (54)] is a sum of two contributions. The first contribution is due to electrostriction, i.e., the deformation of the dielectric under the influence of the electric field. It is proportional to linear susceptibility, which is n^2-1. The second contribution is heating by the light combined with thermal expansion. Heating may result from residual light absorption in the dye solution, e.g., by triplet states of the dye molecules, or from collisional relaxation in dye molecules following stimulated emission (Fig. 1). We attribute the major contribution to the relaxation of dye molecules from the lower laser level to the ground state. The relaxation of the pump excitation to the upper laser level does not contribute to the response function, since it is not correlated with the laser light field. The energy absorbed in

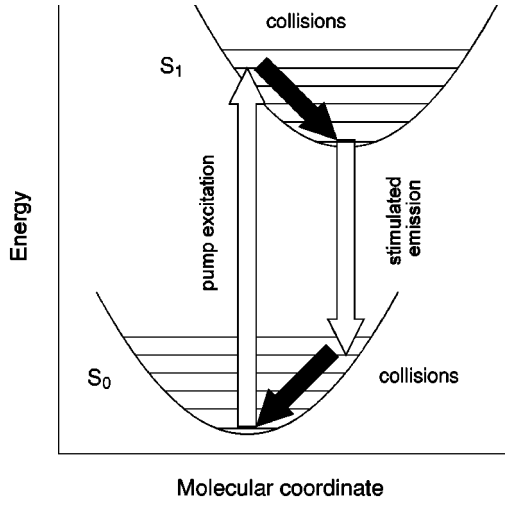

FIG. 1. Energy-level diagram of a dye molecule and schematics of pump excitation, collisional relaxation, and laser emission.

the medium due to relaxation is proportional to both the energy of the amplified laser light and the ratio of the energy of the lower laser level to the laser photon energy. We assume that the energy of the lower laser level is close to the energy excess of the pumped level (pump frequency $\omega_p = 2\pi c/\lambda_p$) over the upper laser level, and write the ''absorption'' coefficient α in Eq. (54) as

$$\alpha \approx \frac{\omega_p - \omega_{ab}}{2\omega_{ab}} B_{\max} N \frac{L}{cl}. \tag{59}$$

The above analysis shows that the response function contains four terms. The first two terms represent stimulated Brillouin (SBS) and Rayleigh (SRLS) scattering due to electrostriction. The second two terms are optothermal contributions defined as stimulated thermal Brillouin scattering (STBS) and stimulated thermal Rayleigh scattering (STRLS). Figures 2 and 3 show the calculated response function of the dye solution for a Rh6G dye laser emitting at 600 nm and with $\lambda_p = 514$ nm. The laser gain $B_{\max}N$ is set at 4% per cavity round trip (equal to the cavity loss). The thickness of the dye jet is $l = 100\ \mu$m, and $w_0 = 6.7\ \mu$m. The dye solvent is ethylene glycol (molar mass 62) with the parameters $n = 1.43$, $\rho_0 = 1110$ kg/m^3, $\nu = 1660$ m/s, $H = 0.019$ kg/ms, $\lambda_T = 0.25$ kg/(s^2 K), and $C_p = 2400$ m^2/s^2 K, all taken from Ref. [26]; and $C_\nu \cong C_p - (T_0\beta_T^2/\rho_0 k) = 2050$ m^2/(s^2 K), $\beta_T = 6.2\times10^{-4}$ K^{-1}, and the compressibility $k = 3\times10^{-10}$ ms^2/kg, all taken from Ref. [27].

The electrostrictive part of the response function is shown in Fig. 2 for three values of $|\mathbf{K}|$ expressed through the angle β between light waves in Eq. (55). It is calculated with Eq. (54) under the assumption that optothermal effects are absent ($\alpha = 0$), and only SBS and SRLS are present. For counterpropagating light waves ($\beta = \pi$) the Brillouin resonance has its maximum value at $\omega_B = \omega_B^{\leftrightarrow} = 2\pi\times 8$ GHz. The spectral width of SBS is $\Gamma_B = 2\pi\times 2.5$ GHz (FWHM). At smaller angles between the light waves (smaller value of $|\mathbf{K}|$), the maximum of the response function becomes higher and narrower, Eq. (56). The contribution of stimulated electrostrictive Rayleigh scattering (SRLS) is very small. It is hardly visible around zero frequency.

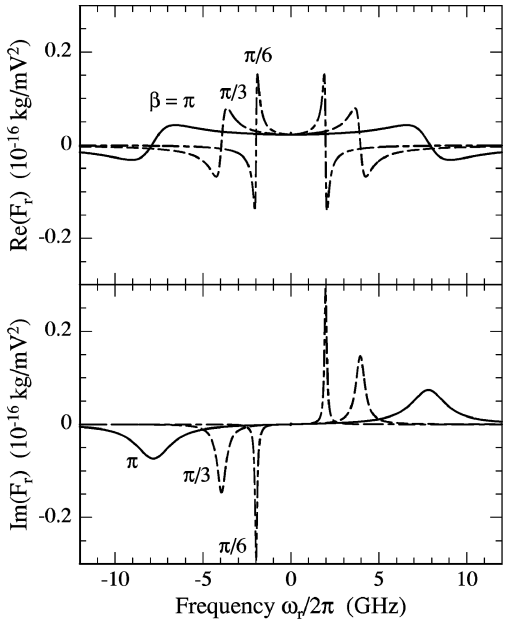

FIG. 2. Response function of the gain medium for excitation of density waves by electrostrictive excitation induced by two light waves that cross at the angle $\beta = \pi$ (solid line), $\pi/3$, and $\pi/6$ (dashed lines).

Figure 3 shows the optothermal contribution of the response function for the same values of $|\mathbf{K}|$ as in Fig. 2. The Brillouin contribution (STBS) has smaller amplitude but larger spectral width than the Rayleigh contribution (STRLS). Therefore the response function is shown on two frequency scales: Fig. 3(a) shows the complete spectrum of STBS, and Fig. 3(b) a narrow section which contains, however, all of the STRLS. The strongest contribution comes from STRLS, but its spectral width is some 10 MHz only. For counterpropagating light waves, e.g., it is $\Gamma_R \cong 2\pi \times 16$ MHz (HWHM).

Figures 2 and 3 show that the contribution of SBS is much larger than that of SRLS and STBS, but the contribution of STRLS, at small frequencies, might be even larger than that of SBS. The relative strength of the influence of the most important contributions, SBS and STRLS, on laser dynamics is estimated when comparing the imaginary parts of the response functions, since these parts are responsible for the variation of the light *amplitudes*. The area under the imaginary part of the SBS resonance curve in Fig. 2 for counterpropagating light waves is approximately three times larger than that under the STRLS resonance in Fig. 3(b). Moreover, the STRLS peak is very narrow and poorly overlaps with the beat notes in lasers of less than 10-m cavity length. Typical dye lasers are much shorter, and we conclude, that FWM by SBS dominates in a multimode dye laser over that by STRLS. Taking into account only SBS, the response function [Eq. (54)] writes

$$F_r(|\mathbf{K}|^2) = \varepsilon_0 \frac{n^2-1}{2} \frac{n^2+2}{3} \frac{|\mathbf{K}|^2}{\omega_B^2(|\mathbf{K}|^2) - \omega_r^2 - i\omega_r \Gamma_B(|\mathbf{K}|^2)}. \tag{60}$$

The scattering coefficient $S^{(\mathrm{SBS})}$ is calculated from this response function by taking into account the distribution of

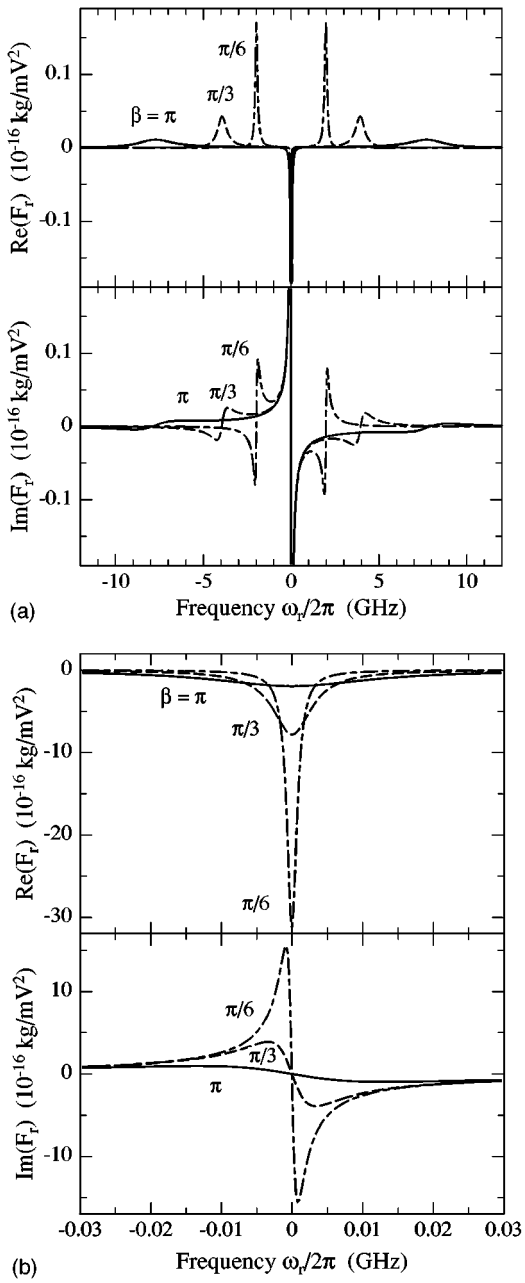

FIG. 3. Response function of the gain medium for excitation of density waves by optothermal excitation induced by two light waves that cross at the angle $\beta=\pi$ (solid line), $\pi/3$, and $\pi/6$ (dashed lines). (a) Contributions from STBS and STRLS; (b) same as in (a), but the frequency scale is expanded, and the ordinate scale compressed.

the light field either for counterpropagating [Eq. (23)] or copropagating [Eq. (24)] waves, using Eqs. (25) and (53):

$$S_r^{(\mathrm{SBS},\leftrightarrow)}=S_{\max}^{\mathrm{SBS}}\,\frac{\omega_B^{\leftrightarrow}}{\omega_r}\,\frac{1+i[(\omega_B^{\leftrightarrow 2}-\omega_r^2)/\omega_r\Gamma_B^{\leftrightarrow}]}{1+[(\omega_B^{\leftrightarrow 2}-\omega_r^2)/\omega_r\Gamma_B^{\leftrightarrow}]^2}, \quad (61)$$

$$S_r^{(\mathrm{SBS},\Rightarrow)}=S_{\max}^{\mathrm{SBS}}\int_0^{\infty}d(|\mathbf{K}|^2)\,\frac{w_0^2}{4}\exp\left(-\frac{w_0^2}{4}\left|\mathbf{K}\right|^2\right)$$
$$\times\frac{i\omega_B^{\leftrightarrow}\Gamma_B^{\leftrightarrow}(c/2n\omega_L)^2|\mathbf{K}|^2}{(\omega_B^{\leftrightarrow 2}+i\omega_r\Gamma_B^{\leftrightarrow})(c/2n\omega_L)^2\mathbf{K}^2-\omega_r^2}. \quad (62)$$

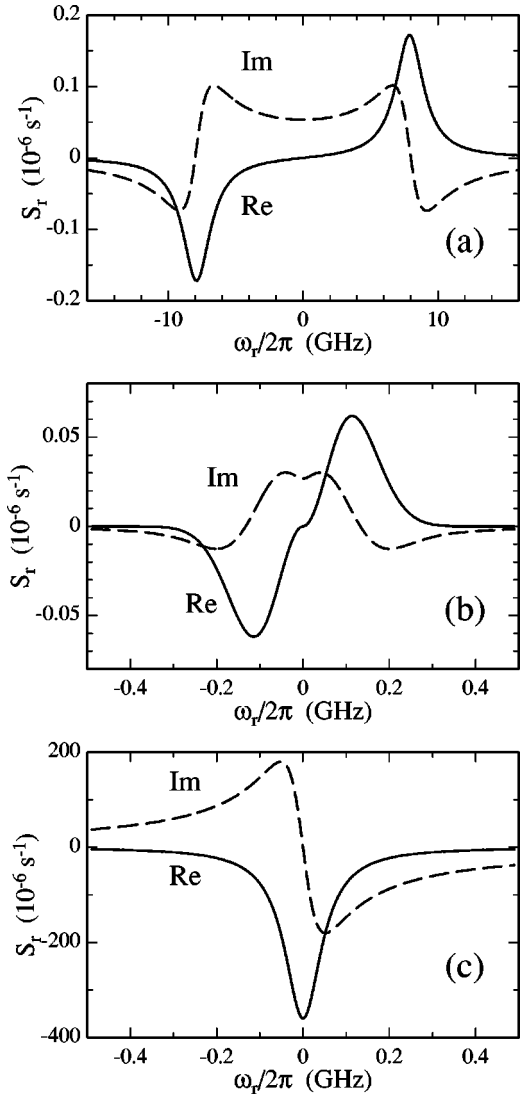

FIG. 4. Scattering coefficients $S_r(\omega_r)$ for SBS in (a) backward and (b) forward direction, and for (c) PP.

In Eqs. (61) and (62),

$$S_{\max}^{\mathrm{SBS}}=\left[\frac{n^2+2}{3}\,(n^2-1)\right]^2\,\frac{\hbar\omega_L^4}{\rho_0 c^2 n^2}\,\frac{2}{\pi w_0^2 L}\,\frac{l}{L}\,\frac{1}{\omega_B^{\leftrightarrow}\Gamma_B^{\leftrightarrow}} \quad (63)$$

is the maximum value of the scattering coefficient. For a laser with cavity length $L=1$ m and with the above parameters, $S_{\max}^{\mathrm{SBS}}=1.7\times10^{-7}\ \mathrm{s}^{-1}$.

The scattering coefficient in the backward direction, $S_r^{(\mathrm{SBS},\leftrightarrow)}$, is shown in Fig. 4(a). Its spectral dependence agrees with that of the response function, shown in Fig. 2 ($\beta=\pi$), except that the real and imaginary parts are interchanged. It shows that each laser mode is efficiently coupled with two groups of modes with frequencies shifted by ± 8 GHz. At the cavity length $L=1$ m these groups consist of about 20 modes.

The spectral profile of the scattering coefficient in forward direction $S_r^{(\mathrm{SBS},\Rightarrow)}$ is shown in Fig. 4(b). Its real part is obtained by analytical evaluation of Eq. (62), and its imaginary part is derived from the real part by the Kramers-Kronig

relations. The maximum value of the spectral profile is about one-third of that for backward scattering, and it is situated at a much lower frequency (0.2 GHz). At the assumed cavity length ($L=1$ m) the emitting modes are coupled efficiently only with their next neighbors.

SBS in the backward direction is three times stronger and couples 20 times more laser modes than SBS in the forward direction. Therefore, its influence on laser dynamics is about 60 times larger. In a linear laser, where both scattering directions are present, we neglect SBS in the forward direction and keep only SBS in the backward direction when simulating laser dynamics.

Figure 4(c) shows the scattering coefficient calculated for PP with Eq. (52). Its maximum value is 10^4 times larger than that for the SBS in the forward direction, and it has approximately the same spectral width. Therefore, in the unidirectional ring laser that lacks SBS in the backward direction, we neglect SBS and consider only PP in the simulations. In a standing-wave laser both SBS and PP must be considered.

III. NUMERICAL SIMULATIONS

The equations of motion of the light amplitudes are combined from Eqs. (42) for the first-order contribution to the amplitude and Eq. (25) for the third-order contribution to the amplitudes; they are

$$\frac{d}{dt}a_q=\frac{B_q\overline{N}-\gamma}{2}a_q+f_q+\tfrac{1}{2}\sum_r\sum_p[S_r^{\leftrightarrow}\xi_{p-q}^{\leftrightarrow}+S_r^{\rightleftarrows}(\xi_r^{\rightleftarrows}-\delta_{r,0})]a_{q+r}a_{p+r}^{*}a_p \tag{64}$$

if narrow-band intracavity absorption is lacking. These equations are solved numerically by taking into account FWM due to PP and/or SBS in the backward direction. Since they contain stochastic forces, they are solved by a Monte Carlo procedure. Equation (41) for the mean value of the inversion is adiabatically eliminated. For the initial condition we adopt a thermal distribution of complex light amplitudes of the cavity modes [28,29], i.e., an exponential distribution of photon numbers and random phases. The calculations were done with finite time increments, whose duration should satisfy the condition $\tau<\eta/\gamma(\eta-1)$ for stability of the coupled equations for laser inversion and total photon number. The random force f_q simulating quantum fluctuations is added at each iteration; it has a two-dimensional Gaussian distribution in the complex amplitude space. The mean value of the added photon numbers is given by Eq. (44). Even after one iteration it exceeds the initial number of thermal photons. Therefore the actual realization of the distribution of photon numbers among the modes in the spectrum of laser emission is determined by the random force rather than by the initial conditions.

The parameters of a real cw dye laser were measured. The waist $w_0=6.7$ μm is estimated from the divergence of the laser light. The loss rate of the cavity is determined from the transmittance of the output mirror (2%), and from the internal cavity loss (2% per cavity round trip), as a function of the cavity length, $\gamma=0.04c/2L$. The gain rate is determined from measurements of the output power at different pump rates and cavity lengths as a function of the cavity length, $B=10^{-10}c/2L$. The dipole dephasing rate, $\gamma_t=1.8\times10^{14}$ s^{-1}, is calculated from the spectral width of the gain, and the pump rate is set to $\eta=1.3$. The lifetime of the upper laser level, $\gamma_a=2.5\times10^8$ s^{-1}, was taken from the literature [30].

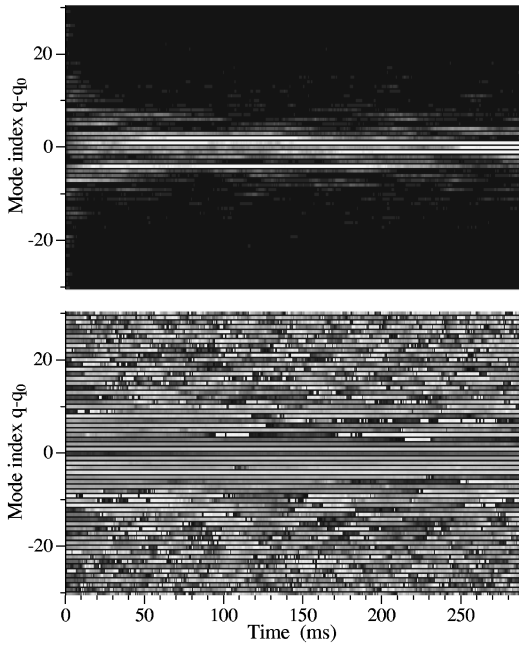

FIG. 5. Simulated trajectories of the light flux (top) and phases (bottom) of the light in individual modes of the laser with quantum fluctuations, but no (nonlinear) mode coupling. Horizontal lines represent individual laser modes; brighter gray values indicate higher power or a more advanced phase (mod 2π). The maximum of laser gain is at $q=q_0$.

The simulated laser has a symmetric two-mirror configuration with an $L=5.25$ cm cavity length (in some cases 1.75 cm). The number of simulated modes is 81, enough for the reproduction of the entire emission spectrum at any time except the first millisecond. This spectral width of the gain corresponds to 10^4 mode spacings (HWHM) at $L=5.25$ cm, and the spectral peak of the SBS coefficient [Eq. (61)] overlaps with the third-neighboring mode.

To speed up computation, we considered SBS phonon frequencies only up to $r=9$. The scattering coefficient according to Eq. (61) decreases quickly with r. For $L=5.25$ cm, it is 30 times smaller at $r=9$ than at $r=1$. This approximation was proved to suffice by observing no deviations from results simulated with the full phonon spectrum.

In contrast, the PP is calculated for all beat frequencies that show up in the laser, i.e., $l<r<80$. Reduction of the beat spectrum may diminish the strength of FWM significantly. This finding is brought about by the imaginary part of the scattering coefficient from a PP, decreasing but slowly with r, as shown in Fig. 4(c).

The results of a numerical simulation of Eqs. (64) in a standing wave, and in a unidirectional ring laser, are shown in Figs. 5–12. Simulated complex reduced amplitudes a_q provide us with photon numbers in laser modes and with the modes' phases. Photon numbers and phases are shown in the figures as two separate trajectories. The increase in brightness of the mode tracks in the trajectories indicates the growth of power or phase. The black background represents

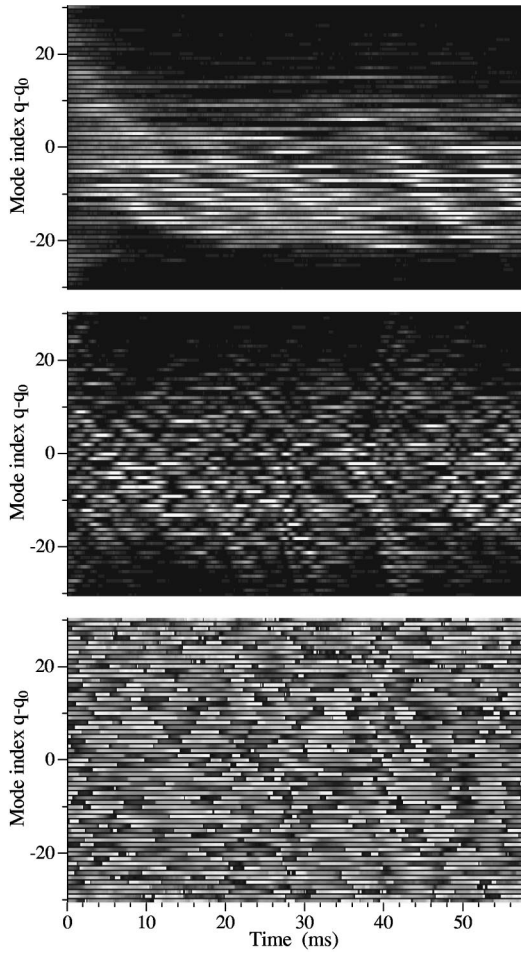

FIG. 6. Simulated trajectories of the light flux in individual modes of the laser with quantum fluctuations and nonlinear mode coupling by degenerate SBS (top), and both degenerate and nondegenerate SBS (center) in a standing-wave symmetric cavity. Phases of the light in individual laser modes with nondegenerate SBS (bottom).

zero photon number and zero phase. The phase is given in the range from 0 to 2π modulo 2π. The length of the trajectories extends from the start of laser oscillation to 290 ms in Fig. 5, and to 58 ms in Figs. 6, 7, and 9–11.

Figure 5 shows the result of a simulation of laser dynamics without nonlinear mode coupling, but with *quantum fluctuations* [Eq. (42)]. The spectral profile of laser emission condenses into a few surviving modes at the end of the track. These modes show, as expected [31], full-scale quantum fluctuations. The autocorrelation time of these fluctuations, that depends upon the average photon number in the laser mode as $t_q = \langle M_q \rangle / \gamma$ [3,31], is about 600 ms in the central laser mode. Weaker modes exhibit shorter fluctuations, but they are hardly visible in the trajectory of photon numbers (top) due to the limited dynamical range of the print. Instead, they are observed in the trajectories of the phase (bottom). The spectral width of the steady-state output, averaged over long time or over many laser pulses, is expected to be merely 1.2 mode separations (HWHM) [3].

The trajectory in Fig. 6 (top) shows the laser dynamics simulated with Eq. (25) at $p = q$, which merely takes into account quantum fluctuations and nonlinear mode coupling only by *degenerate SBS*. This case represents earlier attempts

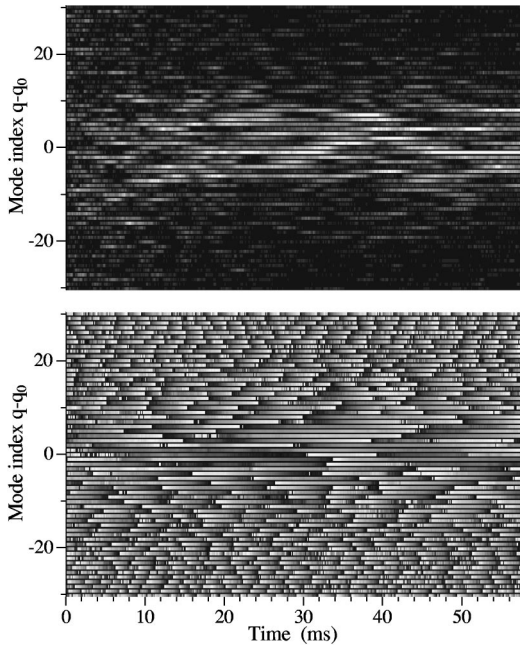

FIG. 7. Simulated trajectories of the light flux (top) and phases (bottom) of the light in individual modes of the laser, with quantum fluctuations and nonlinear mode coupling by PP, in a standing-wave symmetric cavity.

to describe laser dynamics in a ''photon'' approach [16–19]. The main features of this trajectory are (i) the redshift of the emission, which is due to Stokes scattering of photons in the neighboring modes with smaller index, (ii) the emission spectrum being much broader than one without mode coupling, as in Fig. 5 (top), and (iii) the autocorrelation time of the fluctuations being much shorter than expected from the influence of quantum noise only. These features were predicted in previous simulations [16–19].

Figure 6 (center) shows the trajectory of photon numbers in laser modes, simulated with quantum fluctuations and nonlinear mode coupling due to *nondegenerate SBS*. Nondegenerate SBS takes into account the coupling of a larger number of modes, and results in a larger total scattering rate

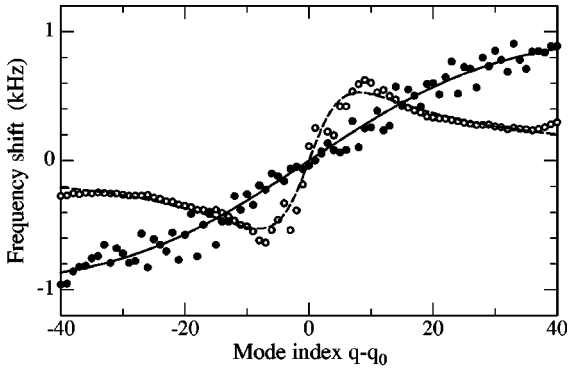

FIG. 8. Closed circles denote the frequency shift of the light in laser modes off the eigenfrequencies of the empty cavity, adopted from the trajectories in Fig. 7 (bottom), which depends upon the mode index, and a fit with Eq. (65) (solid line). Open circles denote the frequency shift of the light in laser modes calculated with Eq. (25) by using a simplified model [32] (degenerate modes $p = q$ only), and fit with Eq. (65) (dashed line).

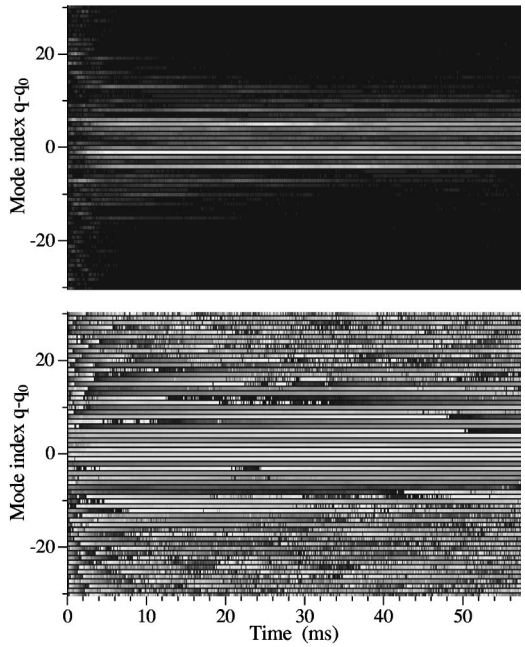

FIG. 9. Simulated trajectories of the light flux (top) and phases (bottom) of the light in individual modes of the laser, with a *unidirectional ring* cavity with quantum fluctuations and nonlinear mode coupling by PP.

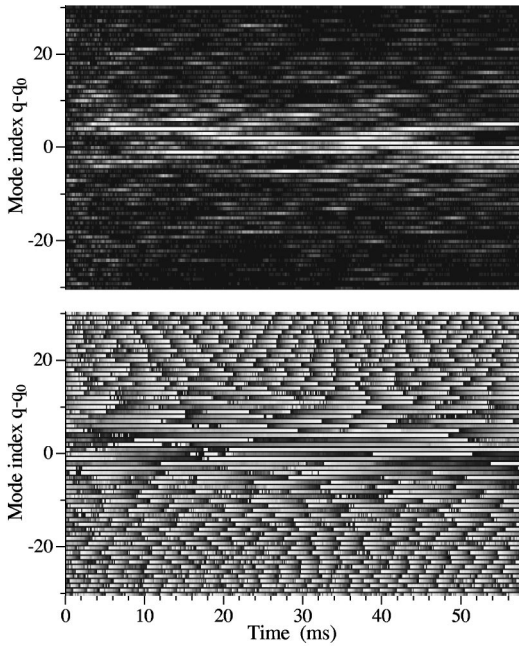

FIG. 11. Simulated trajectories of the light flux (top) and phases (bottom) of the light in individual modes of the laser with a standing-wave symmetric cavity, with quantum fluctuations and nonlinear mode coupling by PP *and* SBS.

than with degenerate SBS. As a result, the spectral broadening turns larger, and the autocorrelation time of fluctuations is shorter than with degenerate SBS. The trajectory shows both a redshift and a blueshift of the output spectrum, but still the redshift dominates. The phases in laser modes shown in Fig 6 (bottom) do not show obvious correlation.

The trajectories in Fig. 7 show laser dynamics, simulated with quantum fluctuations and *nonlinear mode coupling due to PP* in a *standing-wave* symmetric cavity. Now, the emission spectrum is broadened, but not shifted. The autocorrelation time for central modes is larger than before. Phase correlation between adjacent modes is obvious. Moreover, phases permanently increase in the blue half of the spectrum, and decrease in the red: PP push the mode frequencies away from the gain center. This frequency shift is shown in Fig. 8; it is fitted with the dispersive Lorentzian profile

$$\Delta\omega_q = \frac{p_0(q-q_0)}{1+[(q-q_0)/p_1]^2}, \tag{65}$$

with $p_0 = 2\pi \times 32$ Hz and $p_1 = 58$. Such a frequency pushing was predicted theoretically [32] in an attempt to explain measurements of the beat spectrum in a helium-neon laser [33]. The right-hand side of Eq. (25) shows that the frequency shift is caused by the imaginary part of S_r. However, previous models assumed only degenerate terms ($p = q$) to

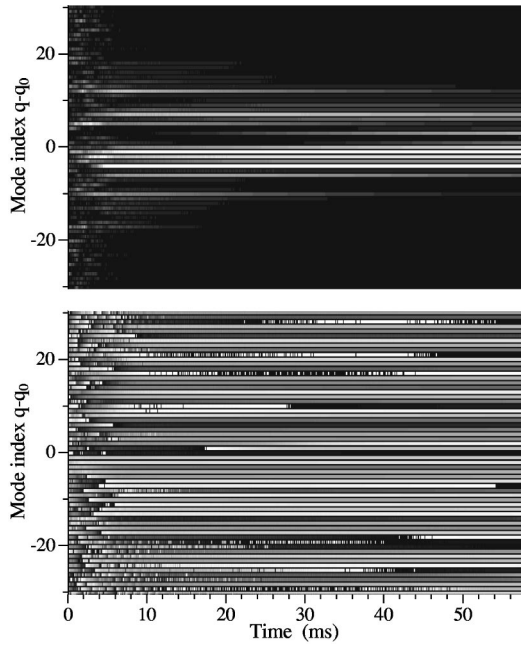

FIG. 10. Simulated trajectories of the light flux (top) and phases (bottom) of the light in individual modes of the laser with a *unidirectional ring* cavity with no quantum fluctuations, but with nonlinear mode coupling by PP.

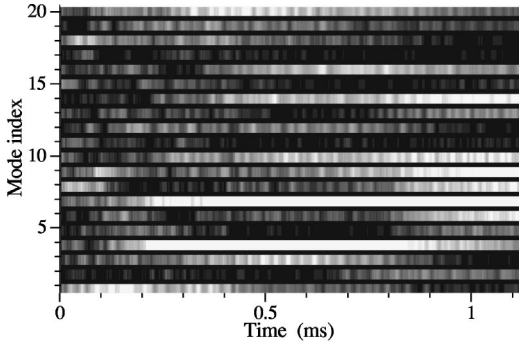

FIG. 12. Section of the trajectory of the light flux in individual laser modes of a standing-wave symmetric laser, simulated with quantum fluctuations and PP. High time resolution.

generate mode pushing. In this case the shift can be derived for modes far from emission center. It is

$$\Delta\omega = \frac{\gamma(\eta-1)\gamma_a}{2(q-q_0)\delta\omega}. \tag{66}$$

The frequency shift calculated with Eq. (25) and assuming the degeneracy of modes p and q, as in that previous model, is also shown in Fig. 8 (open circles) together with its fit (dashed line) according to Eq. (65). The results of this fit, $p_0 = 2\pi \times 129$ Hz and $p_1 = 8$ and 2, differ significantly from those making use of nongenerate mode pairs, though the qualitative features are fairly reproduced. Indeed, the difference originates from previously neglecting nondegenerate terms in the mode coupling by PP. Our results show that this approximation is insufficient for an adequate modeling of multimode lasers.

The trajectories in Fig. 9 show laser dynamics, simulated with quantum fluctuations and nonlinear mode coupling due to PP in a *unidirectional ring* cavity. The autocorrelation time for central modes is significantly longer here than that with the standing-wave laser (Fig. 7), and extends beyond the simulated time range. The phase dynamics shows no obvious mode pushing. In the spectral wings of the emission, disordered and fast-fluctuating phases show up, determined mostly by quantum noise. In the central region, we notice a stable, but nonuniform phase distribution corresponding to phase locking of the laser modes.

Suppression of quantum noise ($f_q = 0$) in a laser with nonlinear mode coupling due to PP in a unidirectional ring cavity enforces amplitude locking of all calculated modes of the laser, which is demonstrated in Fig. 10. Starting from a random distribution, the phases exhibit, after about 5 ms, a quasistable distribution in all the calculated trajectories. This case corresponds to previous approximative simulations of the influence of PP on laser dynamics [10]. The actual laser dynamics with PP and quantum noise shown in Fig. 9 differs, however, from the results of that approximation, and shows that including quantum noise is indispensable.

Simulated laser dynamics with quantum fluctuations and nonlinear mode coupling due to *PP and SBS* in a standing-wave cavity laser is shown in Fig. 11. It resembles the laser dynamics in Fig. 7 calculated for the same laser, but without SBS. Typical features that characterize SBS (Fig. 6, center) are invisible, but mode pushing and phase correlation, typical of laser dynamics with PP, are well reproduced. We conclude that PP *dominate* the laser dynamics of a multimode dye laser even in the standing-wave configuration. This predomination may come about by mode-locking due to PP leading to particular phase relations, which are a handicap for effective FWM by SBS. However, at different values of certain laser parameters, e.g., with smaller cavity loss, the relative strength of SBS might be larger, since the scattering coefficient of the PP is reduced, according to Eq. (52). In contrast, the scattering coefficient of FWM due to SBS does *not* depend on cavity loss. In a unidirectional dye ring laser, where PP is about as strong as in a standing-wave laser, whereas SBS is some 60 times weaker, PP always dominates over SBS.

IV. INTERMODE BEAT NOTES

A. Dynamic eigenvalues of intermode beat notes

Some specific features of the laser dynamics, that may be tested in experiments, require better time resolution of the simulated trajectories. Figure 12 shows a section of such a trajectory with 10-μs time resolution, calculated with Eqs. (64) by taking into account *quantum fluctuations and PP*. The modeled laser consists of a 1.75-cm-long two-mirror linear cavity with the dye jet placed in the center. The pump rate is assumed to be $\eta = 2$, and the cavity loss 4% per round trip. Figure 12 reveals strong pulsations of the photon numbers in individual modes in the frequency range from 10 to 100 kHz. Simulations show this feature neither when dropping all nonlinear terms nor when merely including SBS.

The oscillations are obviously a characteristic feature of the laser dynamics determined by FWM from PP, which is included in Eqs. (64). In order to identify these oscillations we consider, first, a unidirectional ring laser: When inserting the matching values of the spatial correlation functions $\xi_r^{\Rightarrow} = 1$ and $\xi_{p-q}^{\leftrightarrow} = 0$ and transforming Eqs. (64) into equations of motion for photon numbers $a_q^* a_q$, we obtain

$$\frac{d}{dt}(a_q^* a_q) = \frac{\Lambda_q + \Lambda_q^*}{2} a_q^* a_q + (f_q^* a_q + \text{c.c.}) + \sum_{r\neq 0}\left[\left(\sum_p a_{p+r} a_p^*\right)\frac{S_r^*}{2} a_{q+r}^* a_q + \text{c.c.}\right], \tag{67}$$

where the linear loss and quasilinear gain are lumped together in Λ. The strength of FWM described by the last term in Eqs. (67) obviously depends on the correlations $\Sigma_p a_{p+r} a_p^*$ of light amplitudes in the laser modes. These correlations are complex beat notes that should modify the overall laser power at each of the intermode frequencies ω_r. The equations of motion for the beat notes are also derived from Eqs. (64). After suitably rearranging the triple sum, they become

$$\frac{d}{dt}\left(\sum_q a_q^* a_{q+s}\right) = \sum_q \frac{\Lambda_q^* + \Lambda_{q+s}}{2} a_q^* a_{q+s} + \sum_q (a_q^* f_{q+s} + f_q^* a_{q+s}) + \sum_{r\neq 0}\frac{S_{-r} + S_r^*}{2} \times \sum_p a_p^* a_{p+r} \sum_q a_{q+r}^* a_{q+s}. \tag{68}$$

For nonlinearities with spectrally *antisymmetric* scattering coefficient, $S_{-r} = -S_r^*$, such as FWM by SBS [Figs. 4(a) and 4(b)], the last, nonlinear term in Eqs. (68) vanishes. In this case the correlation of light amplitudes in the laser modes is determined only by linear terms and stochastic quantum noise.

Let us consider nonlinear mode coupling with a *symmetric* scattering coefficient, such as with FWM by PP [see Fig. 4(c)], which leaves nonvanishing the nonlinear term in Eqs. (68). The internal sum over q consists of two parts: The first part contains degenerate terms, $r = s$, and represents just the

overall photon number, Eq. (46). It is kept constant due to gain saturation. The remaining sum over p is made up of beat notes, i.e., the variables of Eqs. (68). When keeping only the degenerate terms ($r=s$) in the right-hand-side of Eqs. (68), this equation describes beat notes that undergo damped oscillations,

$$\frac{d}{dt}\left(\sum_q a_q^* a_{q+s}\right)=\frac{(\eta-1)\gamma_a}{B_{\max}}\frac{S_{-s}+S_s^*}{2}\sum_q a_q^* a_{q+s}. \tag{69}$$

The complex eigenvalue of the beat amplitude, i.e., its resonance frequency Δ_s and damping constant Γ_s, is calculated upon substituting the scattering coefficient for PP from Eq. (52),

$$\Gamma_s+i\Delta_s=\frac{\gamma(\eta-1)}{\eta}\frac{1+i\omega_s/\eta\gamma_a}{1+(\omega_s/\eta\gamma_a)^2}. \tag{70}$$

The second part of the internal sum, with nondegenerate terms $r\neq s$, acts as the drive term for the damped oscillator generated by the other beat notes, which adds a deterministic contribution to the drive, but does not modify the eigenvalue.

The oscillation frequency Δ_s of the beat note at intermode frequency ω_s has the same sign as ω_s. Consequently, intermode beating takes place at the frequency $\omega_s+\Delta_s$, which exceeds the frequency separation ω_s of the beating modes. The shift Δ_s of beat frequencies is much larger than found from the dispersion caused by the laser gain, and from simulations with the present model, but with moderate temporal resolution only (Fig. 8). As a result, the sidebands that FWM-PP contributes to the dynamics of light amplitudes in Eqs. (64) are frequency shifted off the mode eigenfrequencies by Δ_s. Mixing these sidebands with the light amplitudes in laser modes gives rise to modulation of the light power with the frequencies Δ_s. These eigenfrequencies of the beat notes are supposed to appear in the photon-number trajectories of the modes. As an example, Fig. 12 shows a section of simulated trajectory with 1-μs time resolution. Indeed, this trajectory reveals light modulation of various frequencies in a 10-kHz range. Fourier analysis yields, in Fig. 13, spectra of the light modulation in the central laser mode q_0 calculated for a 5.75-cm-long laser at pump rate 1.3, and 4% cavity loss per cavity round trip. Figure 13(a), calculated with quantum fluctuations only, but no mode coupling, shows a pure random-walk process. Figure 13(b) shows a spectrum of fluctuations in the output of a mode in a unidirectional ring laser with quantum fluctuations *and* PP. There are several peaks corresponding to the expected eigenvalues. The frequency of these peaks is derived from Eq. (70), which simplifies at $\omega_s \gg \eta\gamma_a$ to

$$\Delta_s=\frac{\gamma(\eta-1)\gamma_a}{\omega_s}. \tag{71}$$

The strongest peak, at $\Delta_1=75$ kHz in Fig. 13(b), is the fundamental pulsation frequency corresponding to the beat-note fundamental frequency $\omega_1=\delta\omega$. Subharmonic pulsations $\Delta_s=\Delta_1/s$ correspond to beat-note overtones $s\,\delta\omega$. Their amplitudes decrease with s increasing.

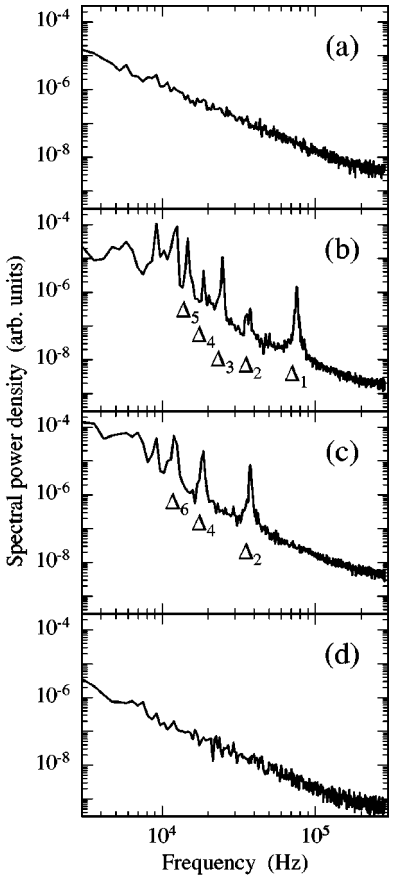

FIG. 13. Spectrum of fluctuations of the light flux in the central laser mode calculated from a simulation of laser dynamics with quantum fluctuations, but (a) no nonlinear mode coupling and (b) with quantum fluctuations and PP, in a unidirectional ring laser, with quantum fluctuations and PP, (c) in a standing-wave laser, and (d) with quantum fluctuations and SBS in a standing-wave laser.

In standing-wave cavities the spatial correlation of modes in Eq. (64) becomes important. A symmetric cavity $z_g=L/2$ has two types of spatial correlations: (i) Correlations of *copropagating* pairs of waves: With the approximation of a thin jet, this correlations function is $\xi_r^{\Rightarrow}=[1+(-1)^r]/2$, such that copropagating pairs of waves contribute to FWM only if the modes are separated by an *even* multiple ($2i$) of the fundamental beat frequency. Accordingly, pulsation frequencies Δ_{2i+1} from odd overtones vanish, as demonstrated in Fig. 13(c). (ii) With correlations of *counterpropagating* pairs of waves, in contrast, $\xi_{p-q}^{\leftrightarrow}=(-1)^{p-q}/2$ holds. Now, the beat notes contain terms like $a_q a_{q+s}$ with alternating signs. Since the correlation is half the value of $\xi_r^{\Rightarrow}$, the dynamic eigenfrequencies Δ_s' have half the values of copropagating pairs, i.e., $\Delta_s'=\Delta_s/2\approx\Delta_{2s}$. Therefore, copropagating and counterpropagating pairs of waves in a standing-wave laser generate only every second modulation frequency, as compared with a ring laser.

Copropagating pairs of waves do not affect the beat notes by antisymmetric FWM (SBS, e.g.) whereas counterpropagating pairs impose a drive on the beat. However, there is no resonance, and the dynamic eigenvalues arise only from symmetric FWM. Figure 13(d) illustrates that statement. It shows a spectrum of photon fluctuations in the laser mode due to quantum fluctuations and FWM due to SBS. As ex-

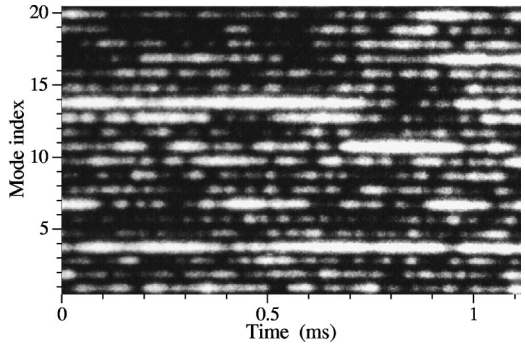

FIG. 14. Experimentally recorded spectrochronogram of the dynamics of the light flux in individual modes of a cw dye laser in a 1.8-cm-long standing-wave cavity.

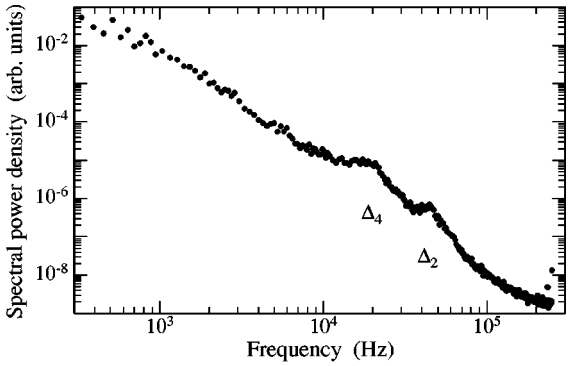

FIG. 15. Fourier spectrum of the power in individual laser modes recorded in the 1.8-cm-long standing-wave cavity at the pump rate $\eta=1.5$.

pected, there are no peaks in it.

The pulsations of the light in individual laser modes have been also observed in experiment. The experimental setup is analogous to one used in previous experiments [8]. A cw dye laser is pumped by an argon laser at $\lambda=514$ nm. A jet of Rhodamine $6G$ dye dissolved in ethylene glycol is set at Brewster's angle to the optical axis in the geometric center of the cavity. Cavity mirrors of 98.75% and 99.95% reflectivity are separated by $L=18$ mm. They form a symmetric, concentric, standing-wave cavity. The rear sides of the mirrors were AR-coated and tilted with respect to the optical axis in order to avoid spectral modulation of the emission spectrum by multiple-beam interferences.

The dye-laser emission is collimated and spectrally analyzed by a 1-m Czerny-Tuner grating spectrograph with 0.005-nm resolution. This resolution suffices for spectrally recording individual longitudinal modes. The spectrograph was used in two modes of operation: as a monochromator, for the observation of the temporally varying emission in individual laser modes by a photomultiplier, or as a polychromator. In the latter version, the laser spectrum is recorded by a diode array or by a mechanical streak camera that allows recording of spectrochronograms with simultaneous temporal and spectral resolution. The streak camera consists of a rotating mirror that replaces the diode array at the output plane of the spectrograph, and of a lens that images the ten-times-magnified laser spectrum on the screen. The moving image is photographed on sensitive 36-mm film (Kodak P3200). The temporal resolution of these spectrochronograms being recorded at 2-Hz rotation of the mirror is about 10 μs. Figure 14 shows a spectrochronogram of a dye laser recorded at the pump rate $\eta=2.0$. It shows strong pulsations of the light power in the laser modes, and resembles the spectrochronogram in Fig. 12, numerically simulated for a dye laser with the same parameters.

The temporal variation of the light flux in individual laser modes is recorded by a photomultiplier with a spectrograph operating in the monochromator mode. Time series with 65 536 data points separated by 2 μs are analyzed by Fourier transformation. The resulting spectrum, shown in Fig. 15, has two distinct peaks at 22 and 45 kHz. Since odd beat frequencies remain unshifted by PP in the symmetric standing-wave cavity ($\Delta_{2i+1}=0$), we assume that these maxima represent even pulsation frequencies at Δ_2 and Δ_4. From these data and the applied pump rate $\eta=1.5$ we derive, with Eq. (71), the total cavity loss of the laser. The obtained value, 2.8% per cavity round trip, complies well with the 1.25% output coupling, if one ascribes 1.55% to the intrinsic loss of the cavity. This value agrees with the results of independent measurements of the cavity loss, 1.5–2 %, in similar lasers when recording the laser threshold vs the transmittance of the output mirror. Note that the experimental line shapes are broadened, a result of nonequidistant mode spacings caused by the dispersion in the cavity. In the above model, however, we assumed equidistant mode spacings according to Eq. (1).

B. Strength of intermode beat notes

It was shown that beat notes of the laser field modes are the driving force for various types of FWM. Now we consider the back action of FWM, by nonlinear mode coupling, on the strength of intermode beating. As shown above, SBS is only a small drive for the beat notes but no damping, whereas PP imposes extra damping and extra driving on them. The last term of Eq. (68) is the nonlinear drive terms of the beat note s. It is a sum of products of two beat notes r and $s-r$. Since the frequency shifts Δ_s of the beat notes vary inversely with $\omega_s=s\cdot\delta\omega$ [Eq. (71)], the shifts Δ_r and Δ_{s-r} do not match Δ_s, and each beat note is driven by the others off resonance. Thus, the extra damping of the beat notes by PP may exceed the extra drive.

Figure 16 shows spectra of beat notes calculated from numerical simulations for a unidirectional ring laser at various moments of time after the onset of laser oscillation. In Fig. 16(a), quantum fluctuations are absent; however, the initial conditions are assumed to be stochastic. The first spectrum at 50 μs shows almost equal amplitudes at all beat frequencies, i.e., the spectrum is characterized entirely by the initial conditions. With increasing duration of laser oscillation the beat notes decrease; they are damped by PP. Furthermore, the extra driving of the beat notes by PP at high frequencies diminishes because the emission spectrum narrows. As a result, high frequencies are damped more than low frequencies.

Figure 16(b) is calculated for the laser with quantum fluctuations present. Here the reduction of beat notes is smaller than in Fig. 16(a), and the stochastic driving force of quantum fluctuations is stronger than that of PP. The stationary beat notes are determined by the balance of this stochastic

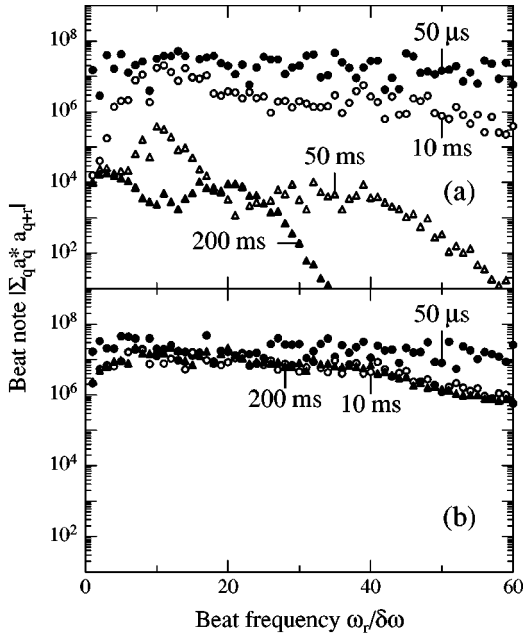

FIG. 16. Spectra of beat notes in simulations of spectral dynamics of a unidirectional ring dye laser when taking into account FWM by PP, without quantum fluctuations (a), and with quantum fluctuations (b), at various times after onset of laser oscillation.

drive of quantum fluctuations and their damping by PP.

This result demonstrates the importance of quantum fluctuations when simulating the laser dynamics and taking PP into account, unlike in a previous model [10]. With quantum fluctuations neglected, PP reduces the beat notes and eventually correlates all the emission spectrum, as observed in Fig. 10. Mode amplitudes are correlated in such a way, that the beat notes are strongly suppressed. As a result, the suppression of beat notes limits the strength of all types of FWM and establishes a stationary amplitude distribution that depends upon initial conditions. Quantum fluctuations act as a permanent driving force for beat notes and establish the stationary level of the beat. With PP present, this stationary level is lower: PP diminishes, via mode coupling, the influence of quantum fluctuations on the phase of the laser modes. An analogous effect takes place in a two-mode He-Ne laser by external modulation at the beat frequency [34].

The influence of PP on the stationary beat spectra is shown in Fig. 17. The beat spectra are averaged over about 10^4 data point in the last 75% section of the simulated trajectories, where stationary laser dynamics is reached. Diagram (a) shows beat notes with quantum noise, but FWM dropped (see Fig. 5). The solid lines in all diagrams of Fig. 17 represent spectra of beat notes with the same photon distribution as in the simulated trajectories, *but with light phases distributed stochastically*. They represent a laser whose spectral dynamics is governed by *quantum noise*, and the photon distribution among the laser modes corresponds to the actual one. With this assumption, beat notes can be calculated from the actual photon distribution for $r \neq 0$, as

$$\left\langle \left| \sum_q a_{q+r}^* a_q \right| \right\rangle = \left(\sum_q M_{q+r} M_q \right)^{1/2}, \qquad (72)$$

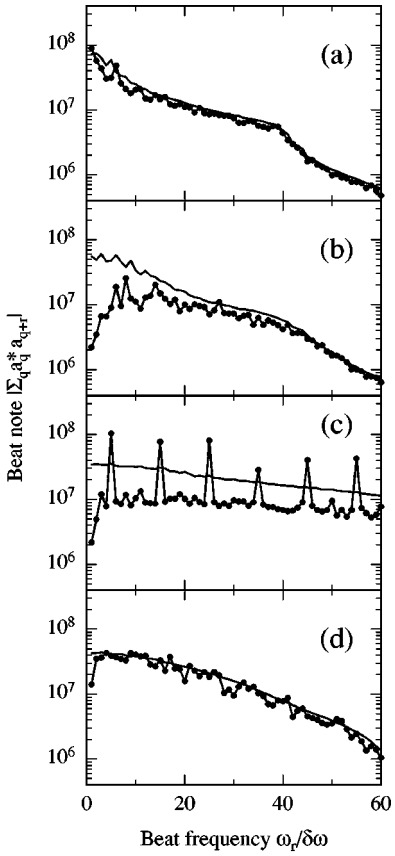

FIG. 17. Stationary spectra of beat notes in simulations of spectral dynamics of a cw dye laser with quantum noise, but no mode coupling (a), with quantum noise and PP, in a unidirectional ring cavity (b), with quantum noise and PP, in a standing-wave asymmetric cavity ($z_g = L/10$) (c), and with quantum noise and SBS in a standing-wave asymmetric cavity ($z_g = L/10$) (d). Solid lines represent spectra of beat notes with stochastically distributed light phases.

This procedure is proved in Fig. 17(a), where the data points are calculated from the left-hand side of Eq. (72), and the line is calculated from the right-hand side of Eq. (72). Since the laser dynamics in this case is governed by quantum noise only, both representations agree with each other.

Figure 17(b) shows simulated beat notes of a laser with *FWM by PP*, and with quantum noise, *in a unidirectional ring cavity* (see Fig. 9). The beat notes (data points) are suppressed, due to the PP, below the level that prevails with comparable emission spectra solely under the action of quantum fluctuations (line).

Figure 17(c) shows beat notes of a laser with FWM due to PP and with quantum noise in a *standing-wave asymmetric cavity*. The gain medium is placed asymmetrically at the position $z_g = L/10$. In a standing-wave laser, the nonuniform spatial mode correlation in the gain medium results in a suppression of the beat notes only between certain pairs of highly correlated modes. The cavity configuration here provides high spatial correlation between every tenth mode. Accordingly, beat notes corresponding to multiples of ten free spectral ranges of the cavity are reduced as compared with beat notes of the laser determined by quantum noise. In contrast, beat notes at the frequencies with no spatial mode correlation ($r = 5,15,25,\ldots$) are even increased.

Obviously, the suppression of beat notes, as it appears with a unidirectional ring laser due to its uniform spatial mode correlation, places restrictions on the relative phases of the field modes, such that phase locking occurs (Fig. 9). With nonuniform spatial correlation of the modes, as it appears in a standing-wave laser, the absence of suppression of certain beat notes provides sufficient freedom for the phases such as to allow mode pushing (Fig. 7). Strong periodic correlation between laser modes in a standing-wave laser might be the basis for regular dynamics, which was observed in earlier experiments [8].

Figure 17(d) shows beat notes in the simulation of the laser dynamics with *FWM by SBS*, and with quantum noise, in the same asymmetric standing-wave cavity. One notes that the beat notes are the same as in the case of dominating quantum fluctuations. This feature proves that SBS does not give rise to mode correlation (also see Fig. 6).

For a measurement of beat notes, Fourier analysis of the recorded total laser output suffices. Since we have to measure beat frequencies between modes separated by a large number of mode spacings, a laser with a long cavity is required in contrast with the experiment on spectrally resolved dynamics. The dye jet was placed in a standing-wave folded three-mirror cavity. The two spherical mirrors with radii of curvature 15 and 30 cm are highly reflecting ($R \cong 99.9\%$). The output plane mirror has 0.4% transmittance. Whereas the position of the jet was set to $z_g = 15$ cm, the cavity length L was varied from 68 to 300 cm. The total laser output was measured with an avalanche photodiode. The beat spectrum was electronically reconstructed from the photodiode signal with a spectrum analyzer (HP 853A/8558B) in the frequency range up to 1.8 GHz.

The spectra of the recorded beat notes (cavity length $L = 300$, 157, and 68 cm) are shown in Fig. 18. The recordings consist of sharp maxima at multiples of the cavity free spectral range, $\delta\omega = 50$ MHz (a), 96 MHz (b), and 220 MHz, respectively. Each maximum corresponds to one beat amplitude. All these spectra show that the beat notes are minimum at multiples of $c/2z_g$, i.e., at 0 GHz, 1 GHz, 2 GHz, etc. These frequencies correspond to separations between modes having a maximum spatial correlation in the dye jet, as expected from the model.

Such a beat spectrum cannot emerge from a periodic interference structure in the emission spectrum, since such a spectral modulation causes *maximum* beat notes at the multiples of the spectral period, not *minimum* ones. The measured beat spectra agree with simulations in Fig. 17(c), and prove that PP dominates the dynamics of the dye laser specified above, correlates the laser modes, and reduces the beat notes.

V. SUMMARY

We have presented the most complete model of a cw multimode dye laser so far. It is based on equations for the complex light field amplitudes in laser modes and takes into account quantum noise and FWM by PP and by various types of stimulated light scattering. Numerical solutions show that SRLS as well as SBS close to the forward direction do not contribute significantly to FWM. However, the electrostrictive part of SBS in the backward direction does

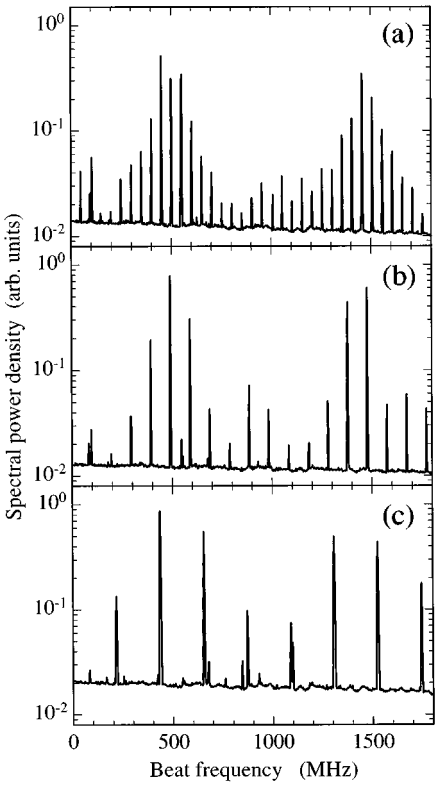

FIG. 18. Experimentally recorded spectra of beat notes in a cw standing-wave dye laser with three different asymmetric cavities: $z_g/L = 0.05$ (a), 0.096 (b), and 0.22 (c). Here z_g is kept constant, and L is varied.

contribute, although less than PP in a typical dye laser. This result is in contrast with that of the simpler ''photon'' approach to SBS, neglecting nondegenerate FWM. The effective inclusion of nondegenerate FWM in our approach allows a consideration of anti-Stokes scattering in addition to Stokes scattering, and enhances the rate of photon scattering events.

FWM by PP and by SBS is distinguished by different spectral symmetry of scattering coefficients with respect to the frequency of the material excitation: the coefficient is symmetric for PP and antisymmetric for SBS. The symmetry of scattering coefficient for PP results in the shift of the nonlinear drive of the beat notes off resonance, and damping the beat notes. In contrast, SBS does not influence mode correlations. The effect of the PP-induced dynamic eigenvalues, i.e., the shift of the beat notes off the multiples of the cavity free spectral range and the suppression of the beat notes, causes mode correlations and self-suppression of FWM, i.e., PP control themselves by negative feedback. However, quantum noise acts as a continuous driving force supporting FWM.

Two characteristic features of the influence of PP on laser dynamics, predicted by the model, have been observed in the experiment: (i) Pulsations of the photon numbers in the laser modes have been detected by recording mode-resolved spectral laser dynamics. (ii) The suppression of the intermode beat notes generated by PP has been proved by Fourier analysis of the records of spectrally integrated output of a laser in a standing-wave cavity configuration. These observations show that PP dominate laser dynamics in dye lasers

with the typical parameters (length, loss, . . .) used in the experiments. However, the relative strength of PP and SBS may change by variation of these parameters. Smaller cavity loss, e.g., reduces the influence of PP and might increase the relative influence of SBS on laser dynamics. Moreover, optothermally excited SRLS might become important with a larger cavity length. Dispersion in the cavity might also become important and should supplement the model. The approach used here for a description of the dynamics of a multimode laser is a prerequisite for a realistic evaluation of the ultimately achievable sensitivity of the emission spectrum of a cw multimode dye laser to intracavity absorption, a problem of superior practical interest.

ACKNOWLEDGMENTS

We thank S. A. Kovalenko for helpful discussions. This work was supported by the Deutsche Forschungsgemeinschaft and, in part, by the Volkswagen-Stiftung.

[1] L. A. Pakhomycheva, E. A. Sviridenkov, A. F. Suchkov, L. V. Titova, and S. S. Churilov, Pis'ma Zh. Eksp. Teor. Fiz. **12**, 60 (1970) [JETP Lett. **12**, 43 (1970)].
[2] T. W. Hänsch, A. L. Schawlow, and P. E. Toschek, IEEE J. Quantum Electron. **QE-8**, 802 (1972).
[3] V. M. Baev and P. E. Toschek, Proc. SPIE **1715**, 381 (1992).
[4] S. E. Vinogradov, A. A. Kachanov, S. A. Kovalenko, and E. A. Sviridenkov, Pis'ma Zh. Eksp. Teor. Fiz. **55**, 560 (1992) [JETP Lett. **55**, 581 (1992)].
[5] J. Sierks, V. M. Baev, and P. E. Toschek, Opt. Commun. **96**, 81 (1993).
[6] V. M. Baev, T. P. Belikova, S. A. Kovalenko, E. A. Sviridenkov, and A. F. Suchkov, Kvant. Elektron. **7**, 903 (1980) [Sov. J. Quantum Elektron. **10**, 517 (1980)].
[7] Yu. M. Aivazyan, V. M. Baev, T. P. Belikova, S. A. Kovalenko, E. A. Sviridenkov, and O. I. Yushchuk, Kvant. Elektron. **13**, 612 (1986) [Sov. J. Quantum Electron. **16**, 397 (1986)].
[8] V. M. Baev, J. H. Eschner, J. Sierks, A. Weiler, and P. E. Toschek, Opt. Commun. **94**, 436 (1992).
[9] M. Sargent III, M. O. Scully, and W. E. Lamb, Jr., *Laser Physics* (Addison-Wesley, Reading, MA, 1974).
[10] S. A. Kovalenko, S. P. Demin, and D. D. Toptygin, Kvant. Elektron. **18**, 451 (1991) [Sov. J. Quantum Electron. **21**, 407 (1991)].
[11] I. McMackin, C. Radzewicz, M. Beck, and M. G. Raymer, Phys. Rev. A **38**, 820 (1988).
[12] R. M. Herman and M. A. Gray, Phys. Rev. Lett. **19**, 824 (1967).
[13] W. Rother, Z. Naturforsch. Teil A **25**, 1120 (1979).
[14] W. Kaiser and M. Maier, in *Laser Handbook*, edited by F. T. Arecci and E. O. Schulz-Dubois (North-Holland, Amsterdam, 1972), p. 1078.
[15] Y. R. Shen, Phys. Lett. **20**, 378 (1966).
[16] Yu. M. Aivazyan, V. M. Baev, V. V. Ivanov, S. A. Kovalenko, and E. A. Sviridenkov, Kvant. Elektron. **14**, 279 (1987) [Sov. J. Quantum Electron. **17**, 168 (1987)].
[17] H. Atmanspacher, H. Scheingraber, and V. M. Baev, Phys. Rev. A **35**, 142 (1987).
[18] Yu. M. Aivazyan, V. V. Ivanov, S. A. Kovalenko, V. M. Baev, E. A. Sviridenkov, H. Atmanspacher, and H. Scheingraber, Appl. Phys. B: Photophys. Laser Chem. **46**, 175 (1988).
[19] V. M. Baev, J. Eschner, A. Weiler, and P. E. Toschek, J. Opt. Soc. Am. B **7**, 2181 (1990).
[20] Yu. M. Aivazyan, V. M. Baev, A. A. Kachanov, and S. A. Kovalenko, Kvant. Elektron. **13**, 1723 (1987) [Sov. J. Quantum Electron. **16**, 1133 (1986)].
[21] D. Pohl and W. Kaiser, Phys. Rev. B **1**, 31 (1970).
[22] R. W. Boyd, *Nonlinear Optics* (Academic, Boston, 1992), Chap. 1.
[23] J. A. Armstrong, N. Bloembergen, J. Ducuing, and P. S. Pershan, Phys. Rev. **127**, 1918 (1962).
[24] A. Yariv, *Quantum Electronics* (Wiley, New York, 1989), p. 399.
[25] M. Lax, IEEE J. Quantum Electron. **QE-3**, 37 (1967).
[26] *CRC Handbook of Chemistry and Physics*, edited by R. C. Weast (CRC, Boca Raton, FL, 1988).
[27] L. Bernstein, *Zahlenwerte und Funktionen aus Physik, Chemie, Astronomie, Geophysik und Technik*, edited by K. Schäfer and G. Beggerow (Springer, Berlin, 1971), Vol. II, Chap. 1.
[28] V. M. Baev, G. Gaida, H. Schröder, and P. E. Toschek, Opt. Commun. **38**, 309 (1981).
[29] V. R. Mironenko and V. J. Yudson, Opt. Commun. **34**, 397 (1980).
[30] A. Penzkofer and Y. Lu, Chem. Phys. **103**, 399 (1986).
[31] S. A. Kovalenko, Kvant. Elektron. **8**, 1271 (1981) [Sov. J. Quantum Electron. **11**, 759 (1981)].
[32] H. Haken and H. Sauermann, Z. Phys. **173**, 261 (1963).
[33] W. R. Bennett, Phys. Rev. **126**, 580 (1962).
[34] I. Steiner and P. E. Toschek, Phys. Rev. Lett. **74**, 4639 (1995).